

Low-Bandgap Porphyrins for Highly Efficient Organic Solar Cells: Materials, Morphology, and Applications

Ke Gao,* Yuanyuan Kan, Xuebin Chen, Feng Liu,* Bin Kan, Li Nian,* Xiangjian Wan, Yongsheng Chen, Xiaobin Peng,* Thomas P. Russell,* Yong Cao, and Alex K.-Y. Jen*

With developments in materials, thin-film processing, fine-tuning of morphology, and optimization of device fabrication, the performance of organic solar cells (OSCs) has improved markedly in recent years. Designing low-bandgap materials has been a focus in order to maximize solar energy conversion. However, there are only a few successful low-bandgap donor materials developed with near-infrared (NIR) absorption that are well matched to the existing efficient acceptors. Porphyrin has shown great potential as a useful building block for constructing low-bandgap donor materials due to its large conjugated plane and strong absorption. Porphyrin-based donor materials have been shown to contribute to many record-high device efficiencies in small molecule, tandem, ternary, flexible, and OSC/perovskite hybrid solar cells. Specifically, non-fullerene small-molecule solar cells have recently shown a high power conversion efficiency of 12% using low-bandgap porphyrin. All these have validated the great potential of porphyrin derivatives as effective donor materials and made DPPEZnP-TRs a family of best low-bandgap donor materials in the OSC field so far. Here, recent progress in the rational design, morphology, dynamics, and multi-functional applications starting from 2015 will be highlighted to deepen understanding of the structure–property relationship. Finally, some future directions of porphyrin-based OSCs are presented.

organic solar cells (OSCs) have attracted significant attention due to their low cost, flexibility, light-weight, semitransparency, and ease of manufacture.^[1–4] The synergistic developments in materials, device design, and morphology have led to increase in power conversion efficiencies (PCEs) of 16.67% and 17.3% for single junction and tandem solar cells, respectively.^[5–10] A key advance has been the use of non-fullerene acceptors. The chemistries available to modify the acceptors hold great promise for pushing this technology into production.

Designing low-bandgap materials has been a focus for maximization of solar energy utilization.^[11] However, few successful donor materials with near infrared (NIR) absorption are well-matched to fullerene derivatives or non-fullerene acceptors, despite the great progress of NIR non-fullerene acceptor materials.^[12,13] Porphyrin, a well-known dye, and its derivatives play significant roles in many bio-

logical processes.^[13] Porphyrin derivatives also show great potential in medicine, photonics, biochemistry, and analytical chemistry, and porphyrin chemistry even becomes an independent discipline.^[12] Furthermore, porphyrin and its derivatives have other

1. Introduction

Developing sustainable energy resources is an urgent need. Among the different solutions that have been developed so far,

Dr. K. Gao, X. Chen, Prof. X. Peng, Prof. Y. Cao
State Key Laboratory of Luminescent Materials and Devices
South China University of Technology
381 Wushan Road, Guangzhou 510640, P. R. China
E-mail: kegao@uw.edu; chxbpeng@scut.edu.cn

Dr. K. Gao, Dr. Y. Kan, Dr. B. Kan, Prof. A. K.-Y. Jen
Department of Materials Science and Engineering
University of Washington
Seattle, WA 98195-2120, USA

Prof. F. Liu
Department of Physics and Astronomy, and Collaborative
Innovation Center of IFSA (CICIFSA)
Shanghai Jiaotong University
Shanghai 200240, P. R. China
E-mail: fengliu82@sjtu.edu.cn

Dr. L. Nian
South China Normal University
Guangzhou 510006, P. R. China
E-mail: nianli@m.scnu.edu.cn

Prof. X. Wan, Prof. Y. Chen
College of Chemistry
Nankai University
Tianjin 300071, China

Prof. T. P. Russell
Polymer Science and Engineering Department
University of Massachusetts
Amherst, MA 01003, USA
E-mail: russell@mail.pse.umass.edu

Prof. T. P. Russell
Materials Sciences Division
Lawrence Berkeley National Lab
Berkeley, CA 94720, USA

Prof. A. K.-Y. Jen
Department of Materials Science and Engineering
City University of Hong Kong
Kowloon, Hong Kong 999077, China
E-mail: alexjen@um.cityu.edu.hk

 The ORCID identification number(s) for the author(s) of this article can be found under <https://doi.org/10.1002/adma.201906129>.

DOI: 10.1002/adma.201906129

inherent advantages making them good candidates for OSCs. First, the wide absorption region and high extinction coefficients can remove thickness constraints on devices, which can enhance the fill factor (FF). Second, their properties can be easily tuned by introducing different functional groups on the meso or β positions of porphyrin, or modification of the central metal ion. Third, the large conjugated plane facilitates the π - π stacking and intermolecular charge transfer, benefitting the charge transport. Finally, the good stability of porphyrin is beneficial for long-term exposure to the sun. Consequently, porphyrins are very promising as NIR materials for OSCs.

We have designed the A- π -Porphyrin (Por)- π -A structure (A indicates electron acceptor unit) with porphyrin or porphyrin derivatives as the core unit, acetylene linkages as the π moieties and different acceptor units as end-groups.^[14] This design integrates not only the inherent advantages of porphyrin, but also has additional advantages. First, the acetylene linkages decrease the dihedral angle between porphyrin and the end-groups, extending the conjugation and facilitating intermolecular π - π stacking. Second, the end-groups can also be tuned to increase the intramolecular charge transfer (ICT) to reduce the optical bandgap (E_g) to broaden the absorption. Third, the optical properties, energy levels, solubility, and morphology can also be fine-tuned by modifying different conjugation lengths and alkyl chains on the porphyrin. Finally, the use of Sonogashira coupling reaction leads to high yield, avoiding the need for dangerous lithium reagents and toxic stannyl intermediates.

Considering these advantages, we also designed and synthesized porphyrins with A- π -Por- π -Por- π -A, A- π -Por- π - π -Por- π -A, or A- π -Por- π -D(A)- π -Por- π -A structures. Careful morphological studies were performed to provide insight for device optimization. A record PCE of 12.06% was achieved using porphyrin-based donor materials for non-fullerene based all small molecule solar cells.^[15] In addition, some other record results have been realized using ternary solar cells,^[16,17] and tandem solar cells,^[18,19] flexible solar cells^[19] and OSC/perovskite hybrid solar cells.^[20] So far, there have been no reviews synthetically discussing the design and synthetic routes, device optimization, applications, morphology, and the related structure–property relationship for porphyrin-based OSCs.^[13] Recent progress especially the rational design of the chemical structures of porphyrins, the morphology dynamics of blend films, and the multi-functional applications of porphyrins will be highlighted here to deepen the understanding of the structure-property relationship.

2. Porphyrin Materials and the Basic Photovoltaic Properties

2.1. Common Synthetic Routes for Porphyrins

There are different approaches to synthesize porphyrin, and porphyrin chemistry has a long history with one century. The synthesis of porphyrin begins with pyrrole, as described in previous reports (Scheme 1a).^[21,22] The pyrrole and formaldehyde with a large excess of pyrrole as a solvent and trifluoroacetic acid as a catalyst were transformed into dipyrromethane.^[21] The product was obtained by reduced pressure distillation with a yield of \approx 65%, and should be stored in the dark in a freezer. The dipyrromethane and aromatic aldehydes with low



Ke Gao is a researcher in the Department of Materials Science and Engineering at the University of Washington with Professor Alex K.-Y. Jen. He received his Ph.D. degree from the State Key Laboratory of Luminescent Materials and Devices, South China University of Technology in 2016 under the guidance of Prof. Yong Cao, Prof. Thomas

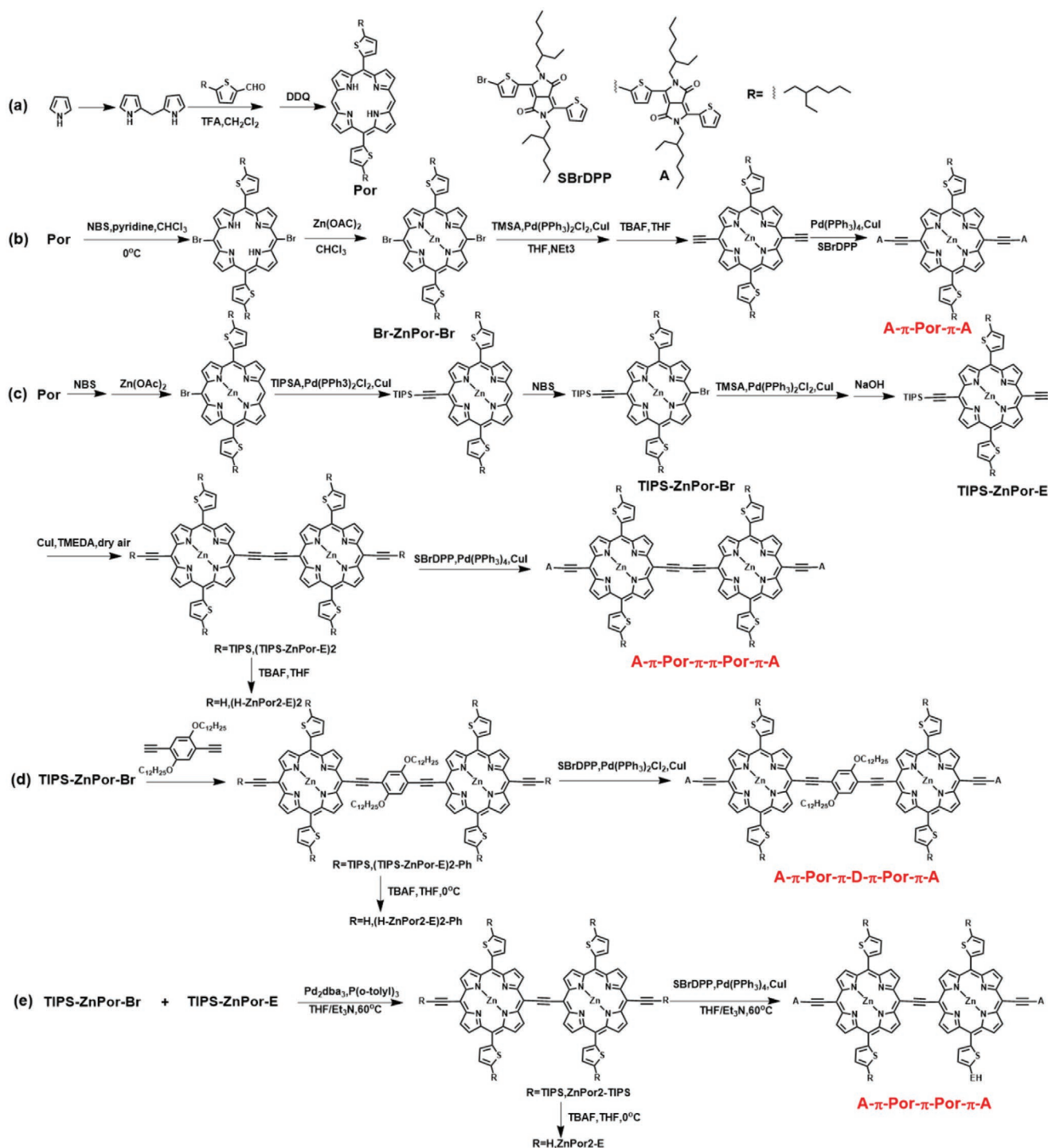
P. Russell, Prof. Xiaobin Peng, Prof. Feng Liu, and Prof. Xiangjian Wan. Currently, his research interest is focused on design and synthesis of organic functional materials for OPV and hybrid solar cells, fabrication, optimization and slot-die printing of OPV devices, and morphology studies of organic electronics.



Alex K.-Y. Jen, chemist, Foreign Member of the European Academy of Sciences. He is serving as the Provost and Chair Professor of the City University of Hong Kong. Before his current post, he served as the Boeing-Johnson Chair Professor and Chair of the Department of Materials Science and Engineering at the University

of Washington. His research interest is focused on utilizing molecular-, polymeric-, and bio-macromolecular self-assembly to create ordered arrangement of organic and inorganic functional materials for applications in photonics, optoelectronics, energy, nanomedicine, and nanotechnology. He has played a pivotal role in starting four companies regarding information technology and energy.

concentrations in methylene chloride can be further cyclized into porphyrinogen with trifluoroacetic acid as a catalyst, then converted into porphyrin after the oxidation of 2,3-dichloro-5,6-dicyano-1,4-benzoquinone (DDQ) with a total yield of 40%. Four types of porphyrin-based materials (A- π -Por- π -A, A- π -Por- π -Por- π -A, A- π -Por- π - π -Por- π -A, or A- π -Por- π -D(A)- π -Por- π -A) can be further designed and synthesized using the porphyrin ring (Scheme 1b–e). All the porphyrin materials shown in **Figures 1** and **2** can be accessed by a similar synthetic route. Thus, we take the synthesis of A- π -Por- π -A as an example. Porphyrin dibromide compound **1** was almost quantitatively obtained in the mixed solvent of chloroform and pyridine by use of two equivalents of N-bromosuccinimide (NBS), pyridine played an important role in preventing side reactions. Compound **1** was then quantitatively converted to Br-ZnPorphyrin-Br. Br-ZnPorphyrin-Br was then coupled with trimethyl silyl acetylene via the Sonogashira



Scheme 1. Synthesis routes for four types of porphyrin derivatives.

reaction in 85% yield, then the trimethyl silyl was quantitatively removed by addition of tetrabutylammonium fluoride to get compound 2. Finally, the compound 2 coupled with the monobromided acceptor unit to get the targeted A-π-Por-π-A in 75% yield. Similarly, the other three types of porphyrin molecules can be synthesized by using the similar reactions for A-π-Por-π-A and the difference is the monobromination of porphyrin. Obviously, all the reactions during the synthesis of the four types of

molecules in Scheme 1 not only avoid the use of the dangerous lithiation reactions and the toxic stannyl intermediates, but also show respectable yields, making the reactions quite eco-friendly. As the purity of the small molecules is of great importance to device performance, the small molecules must be purified as much as possible.^[23] Therefore, the inevitable presence of porphyrin analogues that greatly affect the device performance should be removed by gel permeation chromatography (GPC)

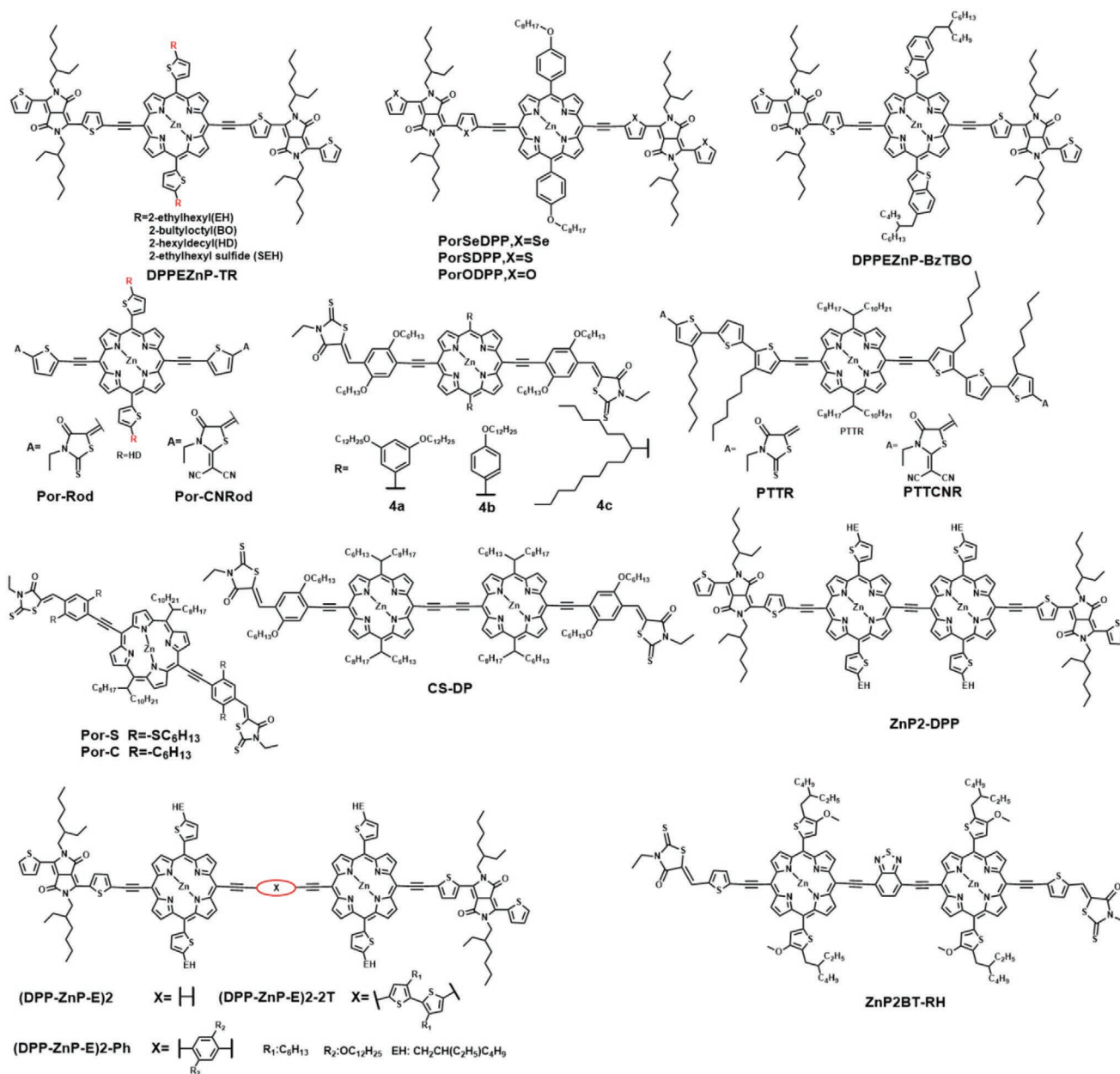


Figure 1. Chemical structures of porphyrin-based materials from our group.

and high performance liquid chromatography (HPLC).^[24] Thus, the purity should reach that of HPLC grade rather than nuclear magnetic resonance (NMR) grade. It should be noted that no impurity was found after being stored in ambient air for three months without shielding for DPPEZnP-TEH despite the existence of ethynylene. The high stability will facilitate their applications in OSCs.

2.2. Photovoltaic Performance of Porphyrins in PCBM-Based Binary Devices

As PCBM was regarded as the only efficient acceptor available before ITIC appeared, the basic photovoltaic performance

of such porphyrins was reflected in PCBM-based binary OSCs. Figure 1 shows the porphyrin materials developed by our group. In 2015, we reported the famous small molecule DPPEZnP-TEH with an A- π -Por- π -A structure in which two ethynylene bridges linked the porphyrin core to two diketopyrrolopyrrole units.^[14] DPPEZnP-TEH has a very broad absorption covering from the ultraviolet (UV) to NIR region and its absorption edge can be extended to 907 nm with a very low E_g of 1.37 eV.^[14] The broad absorption is ascribed to the big conjugation planar of porphyrin and the efficient ICT between porphyrin and DPP units. The acetylene linkages decrease the degrees between porphyrin and DPP units and make DPPEZnP-TEH a planar and facilitate more efficient ICT.

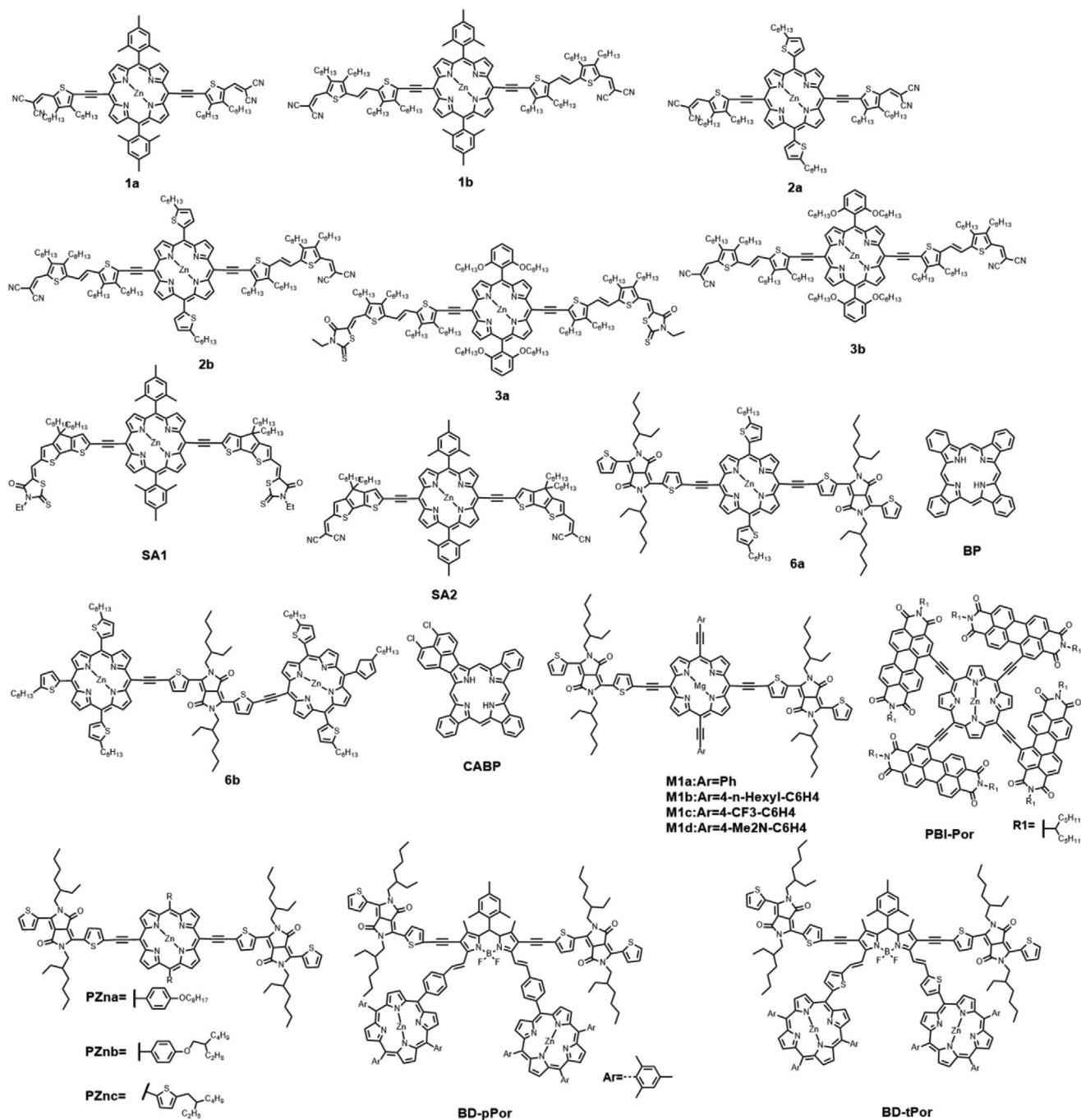


Figure 2. Chemical structures of porphyrin-based materials from other groups.

After optimization with pyridine (Py) and thermal annealing (TA), the devices demonstrated a PCE of 8.08% with a short circuit current (J_{sc}) of 16.76 mA cm⁻² and an external quantum efficiency (EQE) up to 65%. A very low energy loss (E_{loss}) ($E_{loss} = E_g - eV_{oc}$) of 0.59 eV was obtained due to the relatively high open-circuit voltage (V_{oc}) of 0.78 V, and this was the first report of highly efficient OSCs (>8%) with low $E_{loss} < 0.6$ eV.^[14,25,26] It should be noted that the PCE, J_{sc} , and EQE were all the best reported for all OSCs with quite low energy losses.^[14] To fine-tune the crystallinity and further improve the performance

of the devices, a systematic study on the different alkyls attached to the thiophene units from side chains on the porphyrin core was performed. The different molecules with different alkyls show the similar energy levels and absorption profiles because the alkyls do not affect the conjugation. A high PCE of 9.06% with a short circuit current of 19.58 mA cm⁻² was achieved by use of DPPEZnP-TBO and optimization of pyridine (Py) and 1,8- dioctane (DIO) mixture, making them the second series of small molecule with PCE > 9% and the best low-bandgap donor materials in OSC field.^[27]

The morphology studies discussed in Section 3.1 account for the remarkable performance and provide some insight into the formation and optimization of the morphology. The replacement of thiophene on DPP units with selenophene could narrow the band gap because the selenium atom is more polarizable which could facilitate more overlap between the thiophene and adjacent units. We designed and synthesized thiophene, selenophene and furan terminated diketopyrrolopyrrole-based porphyrins (PorSDPP, PorODPP, and PorSeDPP) to study the impacts of different elements from the same main group on the performance of devices.^[28] They showed similar absorption profiles. PorSeDPP showed the smallest E_g of 1.33 eV while PorODPP and PorSDPP showed E_g of 1.38 and 1.36 eV, respectively. However, the optimal PCEs of the devices based on PorODPP and PorSeDPP were much lower than those based on PorSDPP due to the lower FFs and J_{sc} s arising from the poorer morphology.^[28]

With aim to improve the V_{oc} while maintaining the J_{sc} of the DPPEZnP-T series, benzothiophene groups were introduced to the meso positions of porphyrin to construct DPPEZnP-BzTBO because benzothiophene possessed lower electron-donating property.^[29] The devices optimized with pyridine and thermal annealing, followed by solvent vapor annealing (SVA) with chloroform, showed a PCE of 9.08% with a V_{oc} of 0.80 V. The PCE retained 95% of its values for SVA times between 60 and 95 s which would facilitate bulk production due to the large processing window.^[29] In order to further increase the V_{oc} of the devices, we designed a series of porphyrins with 3-ethylrhodanine or 2-(1,1-dicyanomethylene)rhodanine as end-groups because of their lower electron-accepting property than DPP units. Both Por-Rod and Por-CNRod were constructed with thiophenylethynyl as bridges to connect the porphyrin core to the terminal groups.^[30] Por-Rod-based devices with Py + TA presented the best PCE of 4.7% with a very low E_{loss} of 0.53 eV and high EQE over 60%, but Por-CNRod almost did not exhibit photovoltaic response due to the mismatched energy levels.

Considering the aliphatic substituents facilitate the stacking of molecules, three porphyrins with the phenylethynyl moiety as linkages were designed and synthesized to study whether the aliphatic or aromatic peripheral substituents (10,20-bis[3,5-di(dodecyloxy)phenyl] for **4a**, 10,20-bis(4-dodecyloxyphenyl) for **4b**, and 10,20-bis(2-hexylnonyl) for **4c**) are more beneficial to performance of devices.^[31] The stronger intermolecular π - π stacking and higher charge transfer mobility for aliphatic substituent-based porphyrin were translated into the best PCEs of 7.7% and 7.55% for conventional and inverted devices, respectively.^[31] In order to lower their bandgaps to increase J_{sc} of devices, we then replaced the phenyl with 3,3'-dihexyl-terthiophene to get two porphyrin molecules having 2-octylundecyl as peripheral substituents, 3-ethylrhodanine (PTTCNR) or 2-(1,1-dicyanomethylene)-3-ethylrhodanine (PTRR) as end-groups.^[32] The extended conjugation increased the absorption range and enhanced the molecular packing through polymorphism.

After being blended with [6,6]-phenyl-C71-butyric acid methyl ester (PC₇₁BM), the optimized devices based on PTTCNR yielded a PCE of 8.21% while a PCE of 7.66% was obtained based on PTRR.^[32] The alkoxy on the phenylethynyl linkers was then replaced with alkyl and alkylthio to get Por-C and Por-S, respectively.^[33] Por-S based devices demonstrated a PCE of 8.04%, much higher than 5.86% for Por-C-based devices

after optimization with Py + SVA, because Por-S self-assembled to form preferential J-aggregates with PC₇₁BM driven by the S-S interaction from the substituents.^[33]

Different from the porphyrin materials terminating with DPP units, these porphyrins with 3-ethylrhodanine or 2-(1,1-dicyanomethylene)-3-ethylrhodanine showed a limited absorption edge of \approx 850 nm which wasted some solar energy. To circumvent this, two porphyrins with A- π -Por- π -Por- π -A structure were introduced to extend the conjugation and absorption. The porphyrin core in **4c** was replaced with an ethynyl-tethered dimeric porphyrin to construct a new porphyrin CS-DP.^[34] The absorption edge of the targeted molecule further extended to 1100 nm.^[34] After optimization with Py + TA + SVA, the devices blending CS-DP with PC₇₁BM gave a respectable PCE of 8.29% with a high J_{sc} of 15.19 mA cm⁻² and an FF of 70%.^[34] It should be noted that these devices showed extremely low energy losses (<0.43 eV), which is the lowest reported one in the whole OSC field so far.

To further lower E_g and increase the J_{sc} , two new molecules, (DPP-ZnP-E)**2** and ZnP2-DPP with A- π -Por- π -Por- π -A structure, were designed by replacing the 3-ethylrhodanine with diketopyrrolopyrrole (DPP) as terminal units and changing the number of acetylene linkages.^[35,36] In films, both molecules had similar absorption profile and the absorption edge of ZnP2-DPP was red-shifted to 1000 nm because of the enhanced ICT. ZnP2-DPP based devices showed a promising PCE of 8.45% with a remarkable J_{sc} of \approx 20 mA cm⁻², while (DPP-ZnP-E)**2** showed a moderate PCE of \approx 4.5%. The better performance of ZnP2-DPP could be ascribed to the stronger ICT and the more extended photoelectron response.

Attempts were made to improve the performance of (DPP-ZnP-E)**2** by improving its ICT and lowering its bandgap. On one hand, the diethynylene in (DPP-ZnP-E)**2** was replaced with diethynylene-dithiophene and diethynylene-phenylene to get two new porphyrins (DPP-ZnP-E)**2**-2T and (DPP-ZnP-E)**2**-Ph with A- π -Por- π -D- π -Por- π -A structures.^[35] Interestingly, (DPP-ZnP-E)**2**-2T showed a larger E_g than (DPP-ZnP-E)**2** while (DPP-ZnP-E)**2**-2T showed a lower E_g although their Q bands were enhanced. (DPP-ZnP-E)**2**-Ph showed the strongest Q band among the three molecules, indicating the most efficient ICT. As expected, the two new small molecules demonstrated better performance in the devices than (DPP-ZnP-E)**2**. The suitable energy level, strong NIR absorption, and appropriate morphology contributed to the best PCE of 6.42% with a remarkable J_{sc} of 16.34 mA cm⁻² and a V_{oc} of 0.68 V for (DPP-ZnP-E)**2**-Ph based devices.^[35]

Devices based on (DPP-ZnP-E)**2**-2T gave a little lower PCE of 5.5% with a J_{sc} of 13.46 mA cm⁻² and a V_{oc} of 0.79 V.^[35] On the other hand, benzothiadiazole (BT) was introduced as the core of (DPP-ZnP-E)**2** to construct a dimeric porphyrin ZnP2BT-RH with an A- π -Por- π -A- π -Por- π -A structure to further improve the ICT.^[37] In comparison to (DPP-ZnP-E)**2**, ZnP2BT-RH demonstrated higher molar extinction coefficient in the NIR region and a deeper HOMO energy level, increasing both the V_{oc} and J_{sc} . The optimized devices processed with pyridine +SVA gave a very promising PCE of 10.02% with a very low E_{loss} of 0.56 eV. These led to the first binary solar cell based on porphyrin with a PCE > 10%.^[37]

Many other groups also conducted related research to develop efficient porphyrins for OSCs and the representative

materials are summarized in Figure 2. Palomares and coworkers, and Langa and coworkers designed some porphyrin derivatives with dicyanovinylene or 3-ethylrhodanine as end-groups, respectively.^[38,39] Langa group designed two porphyrins with A- π -D- π -A structure in which the central porphyrin unit was linked to the dicyanovinylene groups by one (**1a**) or two (**1b**) thienylenevinylene units, respectively. The absorption edges in both solution and film for **1b** showed obviously redshifted compared with those for **1a**, which was due to the extended conjugation for **1b**.

When blended with PC₆₁BM to fabricate the devices, 1a:PC₆₁BM and 1b:PC₆₁BM showed the PCE of 1.45% and 2.70%, respectively. The authors also used PC₇₁BM to optimize the devices. The resultant **1a**-based devices did not show improvement while the **1b**-based devices achieved an improved PCE of 3.21%. The low performance of **1a**-based devices was ascribed to the low J_{sc} and FF, which was due to the large aggregates in the blend films limiting the exciton dissociation and charge transport.^[39] The same group then replaced the side chains attached the porphyrin with thiophenes to get **2a** and **2b**.^[40]

The devices processed with tetrahydrofuran (THF) based on **2a**: PC71BM and **2b**:PC71BM showed PCEs of 2.75% and 3.18%, respectively. After optimization with pyridine, the PCEs were enhanced to 5.27% and 5.78%, respectively, which resulted from the higher J_{sc} and FF due to the improved crystallinity of the blend films. In addition, the PCEs were further increased to 6.59% and 7.24% after replacement of the hole transporting material PEDOT:PSS with CuSCN, which was ascribed to the increase in V_{bi} and the suppression of the injection of electrons from the anode.^[40] Then they studied and compared the effect of end-groups attached the porphyrins on device performance.^[41]

Two small molecules were designed and synthesized, where the porphyrin core unit was linked to the ethylrhodanine (**3a**) or dicyanovinylene (**3b**) groups via thienylenevinylene-thiophene and ethynylene bridges. After employed in the devices, **3a**-based and **3b**-based devices demonstrated the best PCEs of 5.14% and 6.06%, respectively. The best PCE of 7.63% with a J_{sc} of 13.34 mA cm⁻², a V_{oc} of 0.88 V and an FF of 0.65, was achieved for the devices based on 3b:PC71BM by the optimization of active layers with pyridine and the additional LiTFSI.^[41] They then designed and synthesized two new porphyrins (DPP-ZnP-E)2-Ph SA1 and SA2 by replacement of the bridges with cyclopenta[2,1-b:3,4-b']dithiophene to improve ICT.^[42] After being blended with PC71BM and optimization with DIO, the devices showed reasonable PCEs of 5.82% and 6.80%, respectively. Then devices processed with DIO and SVA gave the best PCEs of 6.71% and 7.93%, respectively. It should be noted that optimal devices based on SA2 demonstrated a low energy loss of 0.55 eV. They then compared the molecular configuration of the A-D-A structure with that of the D-A-D structure, thus designed two molecules **6a** and **6b**, respectively.^[43] The higher J_{sc} and FF, which were ascribed to the stronger π - π intermolecular stacking and more balanced hole- and electron-transport, led to a PCE of 8.03% for **6b**-based devices. In comparison, a PCE of 7.04% was obtained for optimal devices based on **6a**. Nakamura and co-workers reported that tetrabenzoporphyrin and dichloroacene[phtho[q]-tribenzo[b,g,l]porphyrin at a ratio of 75:25 formed a solid solution when blended with PC₆₁BM. The related devices based on the solution showed 3.6% PCE, which

was increased by 16% and 300% compared with those of devices based on single donor component BP and CABP, respectively.^[44] The significant improvements arose from the suitable energy level of the solid solution, due to the electronic coupling of BP and CABP. As magnesium porphyrins are important components in chlorophylls, Matsuo reported four magnesium tetraethynylporphyrin complexes **M1a-M1d** with two aryls as side groups and two DPP units as acceptor groups.^[45] The **M1a** with Ph groups and **M1b** with *n*-hexyl groups demonstrated similar UV-vis absorption profiles. When the electron-donating NMe₂ was used as side groups at **M1d**, the edge of the photovoltaic effect was extended to 1100 nm. The devices based on **M1c** with CF₃ as side groups exhibited the highest V_{oc} of 0.79 V, due to the deeper HOMO level. As a result of the high FF arising from the suitable phase separated morphology, **M1b**-based devices gave the highest PCE of 5.73%. Li and co-workers designed a new tetraethynylporphyrin PBI-Por with perylene bisimide as terminal groups.^[46] Different from the porphyrin donors, they used a porphyrin derivative PBI-Por as a non-fullerene acceptor with PBDB-T as the donor. The new molecule demonstrated good electron mobility, well-matched energy levels and complementary absorption with the donor PBDB-T.^[46] A PCE of 7.4% was achieved after optimization of 1% DIO, showing the great potential of porphyrin for constructing non-fullerene acceptors. Jang and co-workers reported non-fullerene based all small molecule solar cells by blending three porphyrins PZna-c with non-fullerene acceptor IDIC, respectively.^[47] Although the three porphyrins demonstrated similar absorption profiles and energy levels, PZn:a:IDIC blend gave the best PCE of 6.13% due to the most face-on orientations benefitting charge transfer. In order to take the advantage of different dyes, Gros reported two small molecules BD-pPor and BD-tPor in which two DPP units were linked to a BODIPY core by the acetylene linkages and the two porphyrins were also linked to the core by phenyl and thiophene bridges, respectively.^[48] It should be noted that these three units on the targeted molecules possessed complementary absorption. In addition, efficient energy transfer was found between porphyrin and DPP units across the BODIPY unit. After optimization with SVA, BD-pPor:PC71BM and BD-tPor:PC71BM gave a PCE of 6.67% and 8.98% with a low energy loss of 0.63 and 0.50 eV, respectively, indicating that introduction of BODIPY on the porphyrin is a promising strategy.^[48]

It can be summarized that such low bandgap porphyrin derivatives with symmetric structures are arranged by connecting the porphyrin units with electron acceptors and/or electron donors via acetylene linkages. Porphyrins can either be placed in the middle position or at both ends. The donor units can include some fused aromatic rings and the acceptor units are those commonly employed in the OSC field. The acetylene linkages are important in such structures to decrease the dihedral angle between porphyrins and the donor/acceptor units, extending the conjugation and facilitating intermolecular π - π stacking. Such design rule, together with the inherent nature of large planar ring and high degree of conjugation, enabled the absorption of the targeted materials to be extended into NIR region. To design porphyrin materials with lower energy losses, the introduction of polar groups on porphyrin is suggested to enhance its permittivity which can decrease charge transfer excitons binding energy to enhance V_{oc} .^[14,49] It is also useful to

increase the conjugation volumes by introducing acceptor units on the four meso-positions of the porphyrin extending the linear motif to two-dimensions.^[50] Better matched energy levels with low offset between donor and acceptor materials should be also considered for chromophore design. Finally, constructing low bandgap porphyrins with high photoluminescence is another strategy to achieve low energy losses.^[51] In addition, as can be seen from Table 1, porphyrins with rhodanines as end groups usually contribute higher V_{oc} than those with DPP units when applied to the devices. Pyridine is an important additive for the optimization of almost all the porphyrin-based OSC devices, which will be further discussed in the Section 3.1.

3. Morphologies and Dynamics of Porphyrin-Based Devices

3.1. Morphologies of Porphyrin/PCBM Based OSCs

Generating a bulk heterojunction active layer, comprising bicontinuous interpenetrating networks of donor and acceptor domains with domain sizes comparable to the exciton diffusion length, plays a key role in producing high performance OSCs.^[52–54] The interfaces between the domains also require sufficient mixing of donor and acceptor materials to promote exciton dissociation.^[55] However, the domains of the donor and acceptor must provide suitable pathways for efficient charge transport which generally translates into a high degree of order or crystallinity in each phase. In this regard, the perfect morphology should well balance among the crystallinity, the mixing and the phase separation. For porphyrin-based OSCs with PCBM, pyridine is usually used as an additive to optimize the devices.^[27,56] As can be seen in Figure 3b, 4a,f, the as-cast DPPEZnP-TR:PC₆₁BM blend showed a high degree of phase separation resulting from non-favorable interactions between DPPEZnP-TR and PC₆₁BM. It can be seen that the size of domains is ≈ 200 nm, unsuitable for bulk heterojunction (BHJ) morphology. Reducing the size scale of the phase separation is essential.^[27] The formation of morphology has both kinetics and thermodynamic driving forces. By reducing the non-favorable interactions, the driving force for the phase separation can be reduced. While this will not limit the size scale of the phase separation, in the presence of a solvent, the interactions can be mediated. As the solvent evaporates, the two components can be kinetically trapped in a non-equilibrium morphology where the size scale of the domains are small. It is known that pyridine can interact with metalloporphyrin and PCBM as shown in Figure 3c.^[27] Consequently, pyridine can serve two functions. One is to promote solubility in common solvents, thereby, delaying the onset of phase separation between the components. The other is that pyridine can mediate interactions between porphyrin and PCBM, decreasing the driving force of the phase separation, that is, promoting mixing. The transmission electron microscopy image (TEM) (Figure 4b), grazing-incidence X-ray diffraction (GIXD) (Figure 3a) and resonant soft X-ray scattering (RSoXS) (Figure 3b), show that a well-mixed system can be achieved with the addition of pyridine. As seen in Figure 3a,b, and 4c, a suitable bi-continuous morphology can be achieved where the

porphyrin can crystallize, expelling the PCBM from the crystal growth upon thermal annealing. Such morphology yielded good performance.^[14,27] With the addition of DIO, a low vapor pressure solvent for PCBM and non-solvent for the porphyrin, the crystallinity of porphyrin (Figure 3a) and the segregation of the PCBM (Figure 4d) were promoted after chlorobenzene and pyridine are evaporated.^[27] It should be noted that energy-dispersive X-ray spectroscopy (EDX) is used on the HAADF as-cast film to double check its chemical component (Figure 4g–i). It can be concluded from Figure 4f–i that the bright phase is PCBM-rich, which means the black phase is PCBM rich in the bright field TEM (Figure 4a–d). As can be clearly seen from the high-angle annular dark field (HAADF) scanning transmission electron microscopy (STEM), a multi-length scale morphology formed, including porphyrin crystals and PCBM assemblies (Figure 4e) form, which can account for the good performance. This was the first time that a multi-length scale morphology in small molecule solar cells was confirmed from the perspective of both real (Figure 4e) and reciprocal space (Figure 3b). It should be noted that DIO alone cannot reduce the size scale of the phase separation (Figure 3b), due to the preferential interaction with PCBM.

Studies were also performed on the kinetics of the SVA process.^[57] As can be seen from Figure 3e, there are two different change processes for the Py + SVA and Py + TA + SVA processed films. After the well-mixed blend processed with pyridine was exposed to a solvent, the components phase separated due to the enhanced mobility of the system. With time going, the crystallinity enhances and the intensity of the RSoXS increased while the size of the phase separated morphology did not change, that is, q_{max} did not change (Figure 3d,f), indicating that the concentration of PCBM in the PCBM-rich domain was increasing and the concentration of the porphyrin in the porphyrin-rich domain was still increasing. The increasing X-ray contrast/intensity came from the spinodal decomposition. Both the FF and the PCE of the device increased with the domains purifying. However, if the well-mixed blend was processed with thermal annealing and then SVA, two different processes occurred.^[57] The crystallinity decreases before gradually enhances for Py + TA + SVA processed films as can be seen from Figure 3e. The glassy PCBM surrounding the porphyrin crystals stresses the crystals as the porphyrin crystals try to grow, since the annealing temperature is below the T_g of the PCBM. With the introduction of the solvent, the stress is released by the dissolution of the PCBM and porphyrin to promote mixing, as seen in Figure 3g. Then the development of the morphology follows the changes seen with the Py + SVA. Interestingly, the best performance of the devices after optimization by Py + TA, Py + DIO, Py + SVA, and Py + TA + SVA is quite similar. Consequently, these results indicate that it is the crystallization of the porphyrin that dictates the morphology and the performance. The porphyrin crystallization, provided the PCBM is mobile, can direct the sequestration of the PCBM. The BHJ morphology is usually determined by the coupling and competition of crystallization and phase separation and by both thermodynamics and kinetics. As can be seen from Figure 3h, there are many approaches which can tune the kinetics process to optimize the morphology. After careful tune of the parameters, provided that the temperature of thermal annealing, the amount of additives or the time of SVA were

Table 1. Performance of solar cells.

Active layer (Our group)	Optimized condition	E_g [eV]	V_{oc} [V]	J_{sc} [mA cm ⁻²]	FF [%]	PCE [%]	Ref.
DPPEZnP-TEH: PC ₆₁ BM	Py + TA	1.37	0.78	16.76	61.80	8.08	[14]
DPPEZnP-TEH: PC ₆₁ BM	Py + DIO	1.37	0.74	17.5	64.60	8.36	[27]
DPPEZnP-TBO: PC ₆₁ BM	Py + DIO	1.37	0.73	19.58	63.38	9.06	[27]
DPPEZnP-THD: PC ₆₁ BM	Py + DIO	1.37	0.73	17.23	65.54	8.24	[27]
DPPEZnP-THD: PC ₆₁ BM	Py + SVA	1.37	0.74	18.2	70.10	9.41	[57]
DPPEZnP-TBO: PC ₆₁ BM	Py + SVA	1.37	0.77	16.5	62.00	7.90	[57]
DPPEZnP-TBO: PC ₆₁ BM	Py + TA + SVA	1.37	0.78	17.2	63.00	8.50	[57]
PorODPP: PC61BM	PY + TA	1.54	0.81	10.52	50.01	4.26	[28]
PorSDPP: PC61BM	DIO	1.36	0.71	16.00	63.67	7.23	[28]
PorSeDPP: PC61BM	DIO + TA	1.46	0.71	14.93	54.71	5.81	[28]
DPPEZnP-BzTBO: PC ₆₁ BM	Py + TA + SVA	1.40	0.80	16.82	67.54	9.08	[29]
Por-Rod: PC ₇₁ BM	Py + TA	1.47	0.94	12.39	42.71	4.97	[30]
Por-CNrod: PC ₇₁ BM	Py	1.45	0.94	2.43	26.39	0.60	[30]
4a: PC ₆₁ BM	PY + TA	1.60	0.90	7.20	48.12	3.21	[31]
4b: PC ₆₁ BM	PY + TA	1.55	0.90	10.14	55.60	5.07	[31]
4c: PC ₆₁ BM	PY + TA	1.60	0.91	13.32	63.60	7.70	[31]
PTTR: PC71BM	DIO/SVA	1.52	0.80	14.93	64.18	7.66	[32]
PTTCNR: PC71BM	DIO/SVA	1.45	0.82	14.3	70.01	8.21	[32]
Por-S: PC71BM	Py + TA + SVA	1.74	0.91	13.19	66.70	8.04	[33]
Por-C: PC71BM	Py + TA + SVA	1.61	0.87	11.53	58.50	5.86	[33]
CS-DP: PC71BM	PY + SVA	1.26	0.781	15.14	69.8	8.23	[34]
(DPP-ZnP-E)2: PC ₆₁ BM	PY + TA	1.36	0.68	14.37	46.04	4.5	[35]
(DPP-ZnP-E)2-2T: PC ₆₁ BM	PY + TA	1.45	0.79	13.46	51.77	5.5	[35]
(DPP-ZnP-E)2-Ph: PC ₆₁ BM	PY + TA	1.41	0.68	16.34	57.77	6.42	[35]
ZnP2-DPP: PC61BM	TA + SVA	1.28	0.65	19.65	66.15	8.45	[36]
ZnP2BT-RH: PC71BM	Py + SVA	1.40	0.845	17.66	67.15	10.02	[37]
DPPEZnP-TBO: DPPEZnP-BzTBO: PC ₆₁ BM	Py + TA + SVA	1.37	0.78	18.60	70.10	10.17	[62]
DPPEZnP-TEH: PC ₆₁ BM: DPP(TBFu) ₂	TA	1.37	0.79	14.48	62.26	7.12	[61]
DPPEZnP-TEH: PC ₇₁ BM: PTB7	DIO	1.37	0.77	18.94	75.63	11.03	[17]
DPPEZnP-TEH: PC ₇₁ BM: p-DTS(FBTTth ₂) ₂	Py + SVA	1.37	0.79	17.99	77.19	10.97	[16]
DPPEZnP-TEH: PC ₆₁ BM	Py + TA	1.37	0.78	17.01	61.00	8.09	[19]
PTHBDTP: PC71BM/ DPPEZnP-TEH: PC ₆₁ BM	Py + TA	1.37	1.67	9.85	69.00	11.35	[19]
PTHBDTP:PC71BM/ DPPEZnP-TEH: PC ₆₁ BM	Py + TA	1.37	1.63	9.89	63.00	10.16	[19]
DPPEZnP-TBO: PC ₆₁ BM	Py + DIO	1.37	0.74	18.70	64.2	8.92	[18]
DR3TSBDT: PC ₇₁ BM/ DPPEZnP-TBO: PC ₆₁ BM	Py + DIO	1.37	1.60	12.70	62.3	12.70	[18]
DPPEZnP-TSEH: PC ₆₁ BM	Py + DIO	1.38	0.79	17.35	57.1	7.83	[20]
Perovskite/ DPPEZnP-TSEH: PC ₆₁ BM	Py + DIO	1.38	1.04	23.32	78.4	19.02	[20]
Active layer (Other groups)	Optimized condition	E_g [eV]	V_{oc} [V]	J_{sc} [mA cm ⁻²]	FF [%]	PCE [%]	Ref.
1a:PC ₆₁ BM	CB	1.57	0.86	5.72	28.4	1.45	[39]
1a:PC ₇₁ BM	CB	1.57	0.84	5.68	26.6	1.34	[39]
1b:PC ₆₁ BM	CB	1.50	0.82	9.79	35.2	2.70	[39]
1b:PC ₇₁ BM	CB	1.50	0.82	10.83	36.1	3.21	[39]
2a:PC ₇₁ BM	Py	1.48	0.92	10.61	54.0	5.27	[40]
2b:PC ₇₁ BM	Py	1.44	0.86	11.58	58.0	5.78	[40]
2a: PC ₇₁ BM	Py CuSCN	1.48	0.99	10.74	62.0	6.59	[40]
2b:PC ₇₁ BM	Py CuSCN	1.44	0.94	11.67	66.0	7.24	[40]
3a:PC ₇₁ BM	Py/CB	1.54	0.93	10.67	54	5.14	[41]

Table 1. Continued.

Active layer (Other groups)	Optimized condition	E_g [eV]	V_{oc} [V]	J_{sc} [mA cm^{-2}]	FF [%]	PCE [%]	Ref.
3b:PC ₇₁ BM	(Py/CB)/LiTFSI	1.48	0.88	13.34	65	7.63	[41]
SA1:PC71BM	DIO/CB/SVA	1.53	0.85	13.38	59	6.71	[42]
SA2:PC71BM	DIO/CB/SVA	1.45	0.91	13.84	63	7.93	[42]
6a:PC ₇₁ BM	CB + DIO + Py	1.41	0.82	13.41	64	7.04	[43]
6b:PC ₇₁ BM	CB + DIO + Py	1.38	0.82	14.19	69	8.03	[43]
BP:SIMEF2	TA	1.73	0.77	5.9	68	3.1	[44]
CACP:SIMEF2	TA	1.64	0.65	2.5	52	0.9	[44]
BP:CACP:SIMEF2	TA	1.58	0.81	8.3	54	3.6	[44]
M1a:PC ₆₁ BM	Py	1.67	0.74	13.27	49	4.85	[45]
M1b:PC ₆₁ BM	Py	1.69	0.69	14.80	56	5.73	[45]
M1c:PC ₆₁ BM	Py	1.71	0.79	4.61	45	1.65	[45]
M1d:PC ₆₁ BM	Py	–	0.53	12.63	46	3.06	[45]
PBDB-T:PBI-Por	CB/DIO (1%)	1.48	0.78	14.5	66	7.4	[46]
PZna:IDIC	DIO + Py	1.37	0.71	15.46	56	6.13	[47]
PZnb:IDIC	DIO + Py	1.37	0.71	14.03	53	5.21	[47]
PZnc:IDIC	DIO + Py	1.41	0.70	11.46	51	4.08	[47]
BD-pPor:PC ₇₁ BM	SVA	1.52	0.88	12.43	61	6.67	[48]
BD-tPor:PC ₇₁ BM	SVA	1.44	0.95	14.32	67	8.98	[48]

note: Py = pyridine, TA = thermal annealing, CB = chlorobenzene

finely tuned, similar efficiency will be achieved in porphyrin based OSCs.

3.2. Morphologies of Porphyrin/Non-Fullerene Based OSCs

When the porphyrin was used for non-fullerene based OSCs, the morphology will be the other picture.^[15] The pyridine cannot interact with non-fullerene acceptors and the miscibility between porphyrin and non-fullerene acceptors is inherently good due to the similar structure. Thus, we did not employ pyridine to optimize the non-fullerene based OSCs. In our recent case, we blended the DPPEPor-TBO with 6TIC to achieve a best PCE of 12.08%, which is among the best values in the field of non-fullerene based small molecule OSCs. Here, DIO was used, followed by SVA to optimize the morphology. As shown in Figure 5a, the as-cast film demonstrated a poor ordering with an amorphous halo and primary ZnP-TBO signals, suggesting that 6TIC could be trapped or dissolved in the mixture. The mixture formed in the blend is the main reason for different optimized route from PCBM series. As shown in Figure 5b–i, sequentially, the DIO and SVA improved the crystallinity of porphyrin and 6TIC, respectively, leading to the multi-length scale morphology which gave rise to the high performance.^[15]

Interestingly, as can be seen from Figure 5e,f, the peak area of ZnP-TBO increased with SVA under different treatments, suggesting an increase in the crystallinity. There is a good correlation between J_{sc} and the peak area, suggesting the increased crystallinity provided more electron transport channels. It can be concluded that the smaller length scale domains arise from ZnP-TBO, since the J_{sc} is closely related to the interfacial domain area. As can be seen from Figure 5g,h, there is a good

correlation between the π – π stacking peak of 6TIC and the FF of the devices, indicating that SVA enhanced the crystallinity of 6TIC, facilitating electron transport and balanced transport.^[15]

As shown in Figure 5a,i, the result is in good agreement with our predictions that porphyrin and 6TIC mix well and the crystallinity is low. After processing with DIO + SVA, a shoulder in the high q region also appears, indicative of a smaller length scale structure, in addition to the larger structure evidenced by the broad reflection at smaller q . Together, the evidence for a multi-length scale morphology is apparent, which is beneficial for the high performance. In a nutshell, for non-fullerene-based all small molecule solar cells, in addition to the multi-length scale morphology, more attention to improving the crystallinity and electron transport is needed.

4. Applications of Porphyrins in Different Solar Cells

4.1. Ternary Solar Cells

Ternary solar cells are a promising and facile strategy to improve the performance, since the increase in the number of components allows the absorption of solar light over a broader wavelength range.^[16,17,58,59] In addition, the morphology and electrical properties can be manipulated by the introduction of the third functional component.^[16] Low band-gap DPPEZnP-TEH was mixed into the PTB7:PC₇₁BM blend to extend the photo-response and enhance performance. Optimal devices with 30% porphyrin gave the PCEs of 11.03% (certified 10.38%) with a J_{sc} of 18.94 mA cm^{-2} , an FF of 75.63% and a V_{oc} of 0.77 V, making it the best ternary solar cell at that time.^[17]

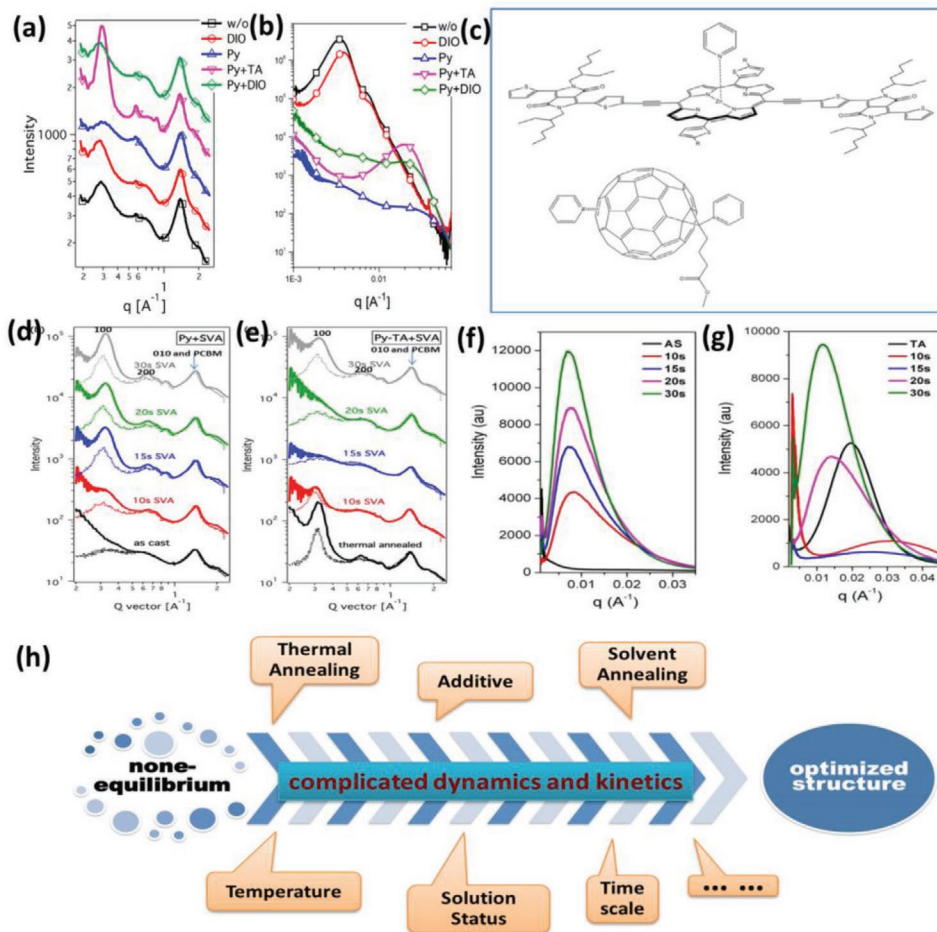


Figure 3. a) GIXD and b) RSoXS of DPPEZnP-TR:PC₆₁BM blend films under different conditions. c) The schematic diagram of the interaction between pyridine and PCBM, pyridine, and porphyrin. Line cut profiles of GIXD and RSoXS of DPPEZnP-TR:PC₆₁BM under d,f) Py + SVA and e,g) Py + TA + SVA. k) schematic diagram of morphology optimization. (a–c) reproduced with permission.^[27] Copyright 2016, Wiley-VCH. (d–g) reproduced with permission.^[57] Copyright 2016, Elsevier.

The high J_{sc} was attributed to the complementary absorption (Figure 6a) and the enhancement of photovoltaic response in NIR region (Figure 5c). The addition of DPPEZnP-TEH and the employment of photo-conductive cathode interface contributed increased the charge extraction and decreased the charge recombination, leading to the enhanced J_{sc} and FF.^[60] It should be noted that the performance was improved over a broad range of DPPEZnP-TEH composition (10–70%) (Figure 6b), a large processing window, which is beneficial for large scale production. Subsequently, we applied the ternary blend strategy in small molecule solar cells, achieving a record-high PCE of 11%, by blending a highly crystalline *p*-DTS(FBTTh2)2 (Figure 6d) with a complementary absorption DPPEZnP-TEH, and low crystallinity PC₇₁BM.^[16] As shown in Figure 6e, the addition of the third component significantly improved the performance. The greater charge transport after the addition of the third highly crystalline component contributed to a higher FF, and the complementary absorption and extended photo-response in NIR region (Figure 6f) yielded the high J_{sc} . Both contributed to the high performance showing that higher performance devices can be achieved by balancing different materials with structural

properties.^[16] Host–guest donors (a donor with high crystallinity and the other with complementary absorption (Figure 6g)) mixed with PCBM were found to yield a favorable morphology. As can be seen in Figure 6h, the DPPEZnP-TEH:DPP(TBFu)₂ blend films demonstrated a new emission peak at ≈ 1010 nm which is red-shifted compared with emission peaks for DPPEZnP-TEH and DPP(TBFu)₂, indicating an exciplex emission.^[61] The interactions on the molecular level was evidenced by the missing of the original emission peaks of the two donors in the blend. The exciplex emission was enhanced after adding 50% DPP(TBFu)₂. The ternary solar cells showed an improved PCE of 7.1% due to the enhanced J_{sc} and FF after adding 10–20% DPP(TBFu)₂ (Figure 6i), underscoring the importance of manipulating the interactions between the different components. After the low loading of low guest donor loading, both the crystallinity and domain purity improved while maintaining a small phase separation which suppressed bimolecular recombination and thus improved the PCE. Using two porphyrins DPPEZnP-TBO and DPPEZnP-BzTBO with the same conjugation structure as donors, ternary solar cells were fabricated with PC₆₁BM.^[62] As shown in Figure 6j, the HOMO levels of DPPEZnP-TBO and

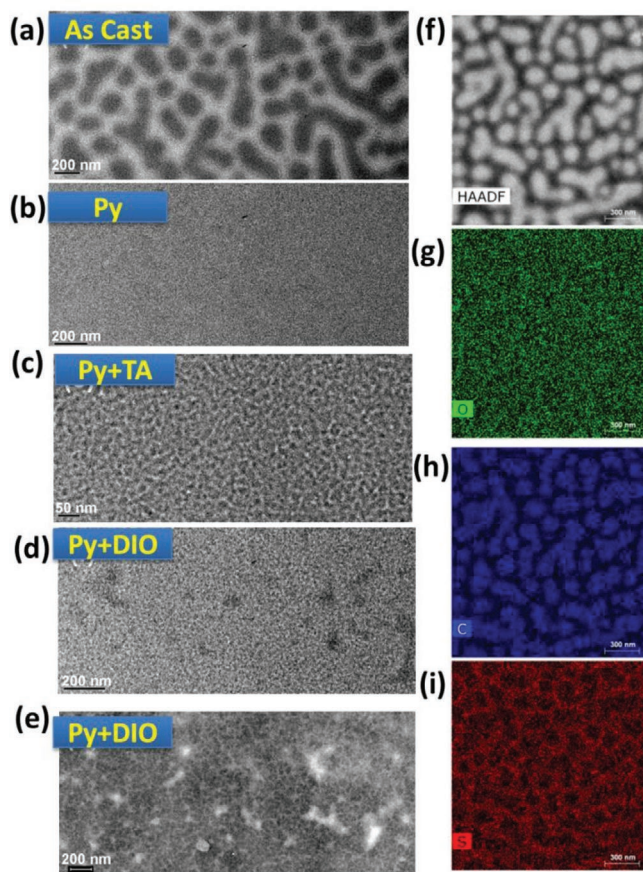


Figure 4. a–d) TEM pictures for DPPEZnP-TR:PC₆₁BM under different conditions. e) HAADF STEM picture for DPPEZnP-TR:PC₆₁BM with pyridine and then DIO. f) HAADF STEM picture for as-cast blend. g–i) EDX EDX mapping of the as-cast blends. Reproduced with permission.^[27] Copyright 2019, Wiley-VCH.

DPPEZnP-BzTBO were -5.18 and -5.26 eV, respectively, but those of the blend films gradually increased with the addition of DPPEZnP-TBO, further indicating good mixing between both porphyrins. As shown in Figure 6k, the performance was increased to 10% for ternary blend in comparison to 9% for the binary blend. The addition of the second donor with the same conjugation structure and a higher HOMO level improved the charge transportation due to the hole relay process, which was the main reason for the improvement of PCE in this example. In a nutshell, all these examples demonstrated that the addition of third component with complementary absorption, balanced crystallinity, and appropriate energy levels are quite crucial for ternary solar cells although the specific roles of the third component are quite different in different ternary solar cells.

4.2. Tandem Solar Cells

Tandem solar cell usually includes two or more sub cells, a front cell absorbing the solar photons in the short wave-length region and a back cell absorbing the solar energy in the long wave-length region.^[18,19,63] Due to the natural low-bandgap NIR absorption characteristics of some porphyrins, they are good

candidates for use in the back cell. In 2016, a tandem OSC shown in Figure 7a was prepared with PThBDTP : PC71BM for the front cell, DPPEZnP-TEH : PC61BM for the back cell and a new configuration of PF3N-2TNDI/Ag/PEDOT:PSS for the interconnecting layer. Figure 7b shows the changes in the $J-V$ curves as a function of the thickness of front and back cells. The J_{sc} was more sensitive to the thickness of the front cell but V_{oc} and FF were more sensitive to the thickness of the back cell. A PCE of 11.35% was achieved under 1 sun after optimizing the thicknesses of the layers (Figure 7b).^[19] As shown in Figure 7c, photons below 650 nm were absorbed by the front cell with the maximum photo-response of 63.2% at 630 nm. A relatively low ratio of photons in the visible range and a high ratio of photons within NIR region were absorbed by the back cell, underscoring the importance of the complementary absorption of the front-cell and the back-cell active layers. Flexible tandem OSCs were also fabricated with PCEs > 10% was achieved, which was the best flexible OSCs at then (Figure 7d).^[19] Preliminary results on the stability of the devices with encapsulation showed that the PCE remained over 90% after 30 days of storage. Small molecule tandem solar cells (Figure 7e) were fabricated, in which DR3TSBDT and DPPEZnP-TBO with complementary absorption were used as donors in front and back sub-cell, respectively. A PCE of 12.7% (certified) was achieved after optimization, which was the record of PCE in the whole field of OSCs (Figure 7f).^[18] As shown in Figure 7g, the EQE demonstrated complementary photo-response from the two sub-cells, accounting for the high J_{sc} . These results reflect the progresses made with tandem solar cells using low-bandgap porphyrin materials.^[5] For optimal tandem solar cells, materials with complementary absorption, an effective interconnecting layer between sub-cells, and the control of active layer thickness must be controlled to achieve higher performance.

4.3. Hybrid Solar Cells

The photo-response of highly efficient perovskite solar cells (PVSCs) is usually limited to about 800 nm, preventing the utilization of NIR solar light, which is a bottleneck for the further performance enhancement of PVSCs. A tandem strategy is costly and the Sn-containing PVSCs with extended photo-response are unstable. Considering the complementary absorption of porphyrins and the well matched HOMO levels with the valance bands of perovskites, the hole transporting layers in PVSCs were replaced with a DPPZnP-TSEH:PC61BM blend to produce a simple OSC-PVSC hybrid solar cell with higher performance (Figure 8a).^[20] As shown in Figure 8b, by optimization of the ratio of DPPZnP-TSEH to PC₆₁BM, and the morphology with binary additives, a similar V_{oc} of 1.04 V, a higher J_{sc} of 23.32 mA cm^{-2} and an FF of 78.4% were obtained, yielding a record-high PCE of 19.02%. This PCE value was greater than that of the conventional perovskite counterpart with a PCE of 18.3% and is still the record in such hybrid solar cells. Figure 8c shows the extended photo-response due to the BHJ layer and Figure 8d shows that the difference in EQEs between the PVSCs and hybrid solar cells agreeing well with the absorption of porphyrin within NIR region, further confirming the efficacy of OSC-PVSC hybrid strategy. More suitable organic materials

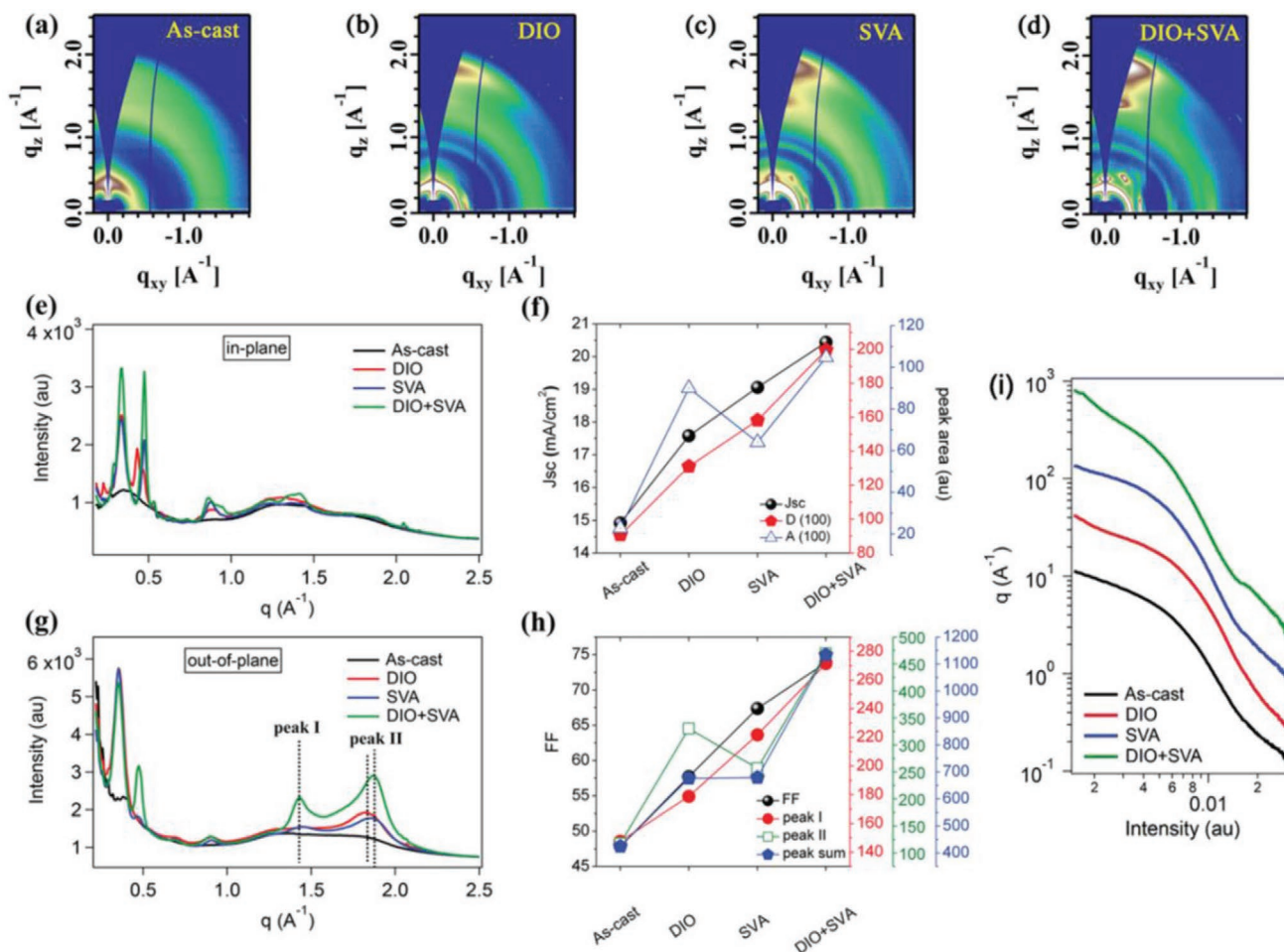


Figure 5. a–d) GIXD diffraction grams of the blend films. e) In-plane line cut profiles of the blend films. f) J_{sc} versus the 100 peak area of donor and acceptor films. g) Out-of-plane line cut profiles of the blend films. h) FF versus the peak I, peak II and the peak sum of the blend films. i) RSOXS profiles of BHJ thin films. All panels reproduced with permission.^[15] Copyright 2019, Wiley-VCH.

with well-matched energy levels and complementary absorption, as well as more effective morphology control, for BHJ layer should be developed for realizing higher efficiency OPV/PVSC hybrid solar cells. The easy-processing and high performance will encourage more work on the OPV/PVSC hybrid solar cells to break through the current PCE limits if rational materials and optimized morphology can be available.^[20]

4.4. Mechanistic Studies

Non-fullerene acceptors bring great hope to the OSC field due to the controlled absorption and energy levels.^[64–69] PCEs have markedly increased to almost 16%.^[6,70] Small molecule solar cells, having components with well-defined chemical structures and molecular weights, overcome batch-to-batch variations typically encountered with polymer-based solar cells.^[71–73] Recently, we used two small molecules ZnP-TBO (DPPEZnP-TBO) and 6TIC with suitable energy levels and complementary absorption, as shown in Figure 9a,b, to fabricate non-fullerene small molecule solar cells (NFSMSCs). Usually, NFSMSCs could not show high PCEs comparable to those of polymer solar cells

which might be due to the high miscibility between small molecule donor and NFAs arising from similar chemical structures. The big planar from porphyrin makes it distinct from other small molecule donors which could decrease the miscibility with NFAs and provide more space to tune the crystallinity and the overall morphology. Then, the use of DIO with SVA enabled the optimization of the blend films, increasing crystallinity and facilitating the formation of a multi-length scale morphology (see Section 3.2). In addition, charge mobility and charge extraction were enhanced with suppressed non-geminate recombination. All of these improved FF and J_{sc} led to a PCE of 12.08% (Figure 9c).^[15] Figure 9d shows the EQE profiles under different treatments and DIO and SVA treatment promoted a high photo-response from the UV to NIR. In the non-fullerene based small molecule solar cells, the main aim for the morphology control is to improve the crystallinity of the small molecules in the blend films. SVA is a quite efficient way to enhance the mobility of the molecules. In addition, it can enhance the crystallinity of the small molecules and increase the domain purity. For materials, compared with other small molecule donors, porphyrin derivatives possess lower miscibility with non-fullerene acceptors thus demonstrate great potential in such devices. The

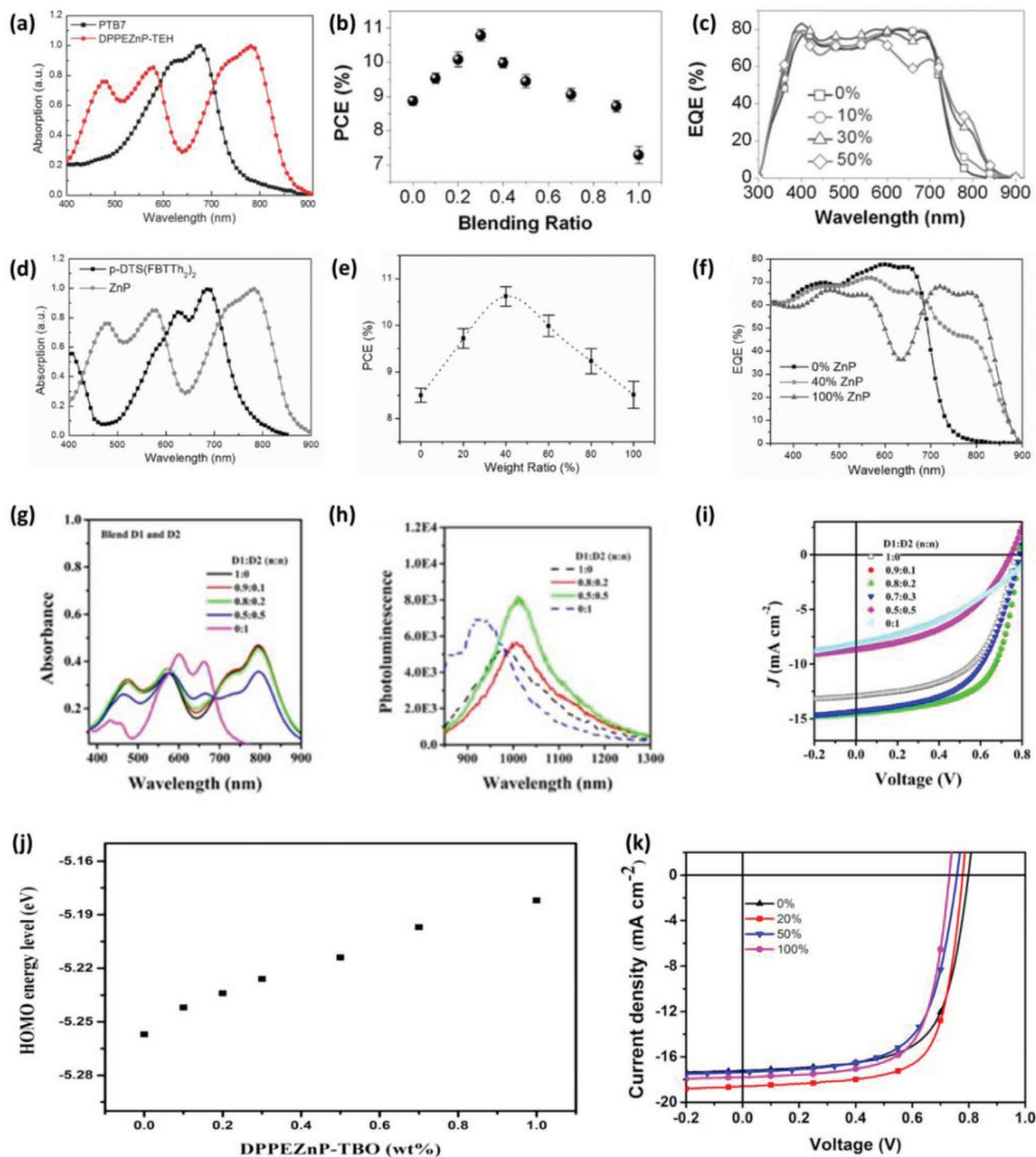


Figure 6. a,d) UV-vis absorption profiles. b,e) PCE versus blending ratio profiles. c,f) EQE profiles for PTB7:PCM:DPPEZnP-TEH blend. g) UV-vis absorption and h) PL profiles of DPPEZnP-TEH (D1):DPP(TBFu)₂ (D2) blend with different ratios. i) *J*-*V* characteristics of the ternary OSCs. j) HOMO energy levels of DPPEZnP-BzTBO, DPPEZnP-TBO, and their blends with different DPPEZnP-TBO loadings. k) *J*-*V* curves of the ternary solar cells with different DPPEZnP-TBO incorporations. (a-c) reproduced with permission.^[17] Copyright 2016, Wiley-VCH. (d-f) reproduced with permission.^[16] Copyright 2017, Wiley-VCH. (g-i) reproduced with permission.^[61] Copyright 2017, Wiley-VCH. (j,k) reproduced with permission.^[62] Copyright 2016, American Chemical Society.

crystallinity of porphyrins should be taken into consideration as an important factor in the future design. Thus, shorter alkyls or fluorine atoms are suggested to be introduced to the porphyrins

to enhance the crystallinity and to further increase their miscibility with non-fullerene acceptors. Consequently, a synergistic development of more suitable donor and acceptor material

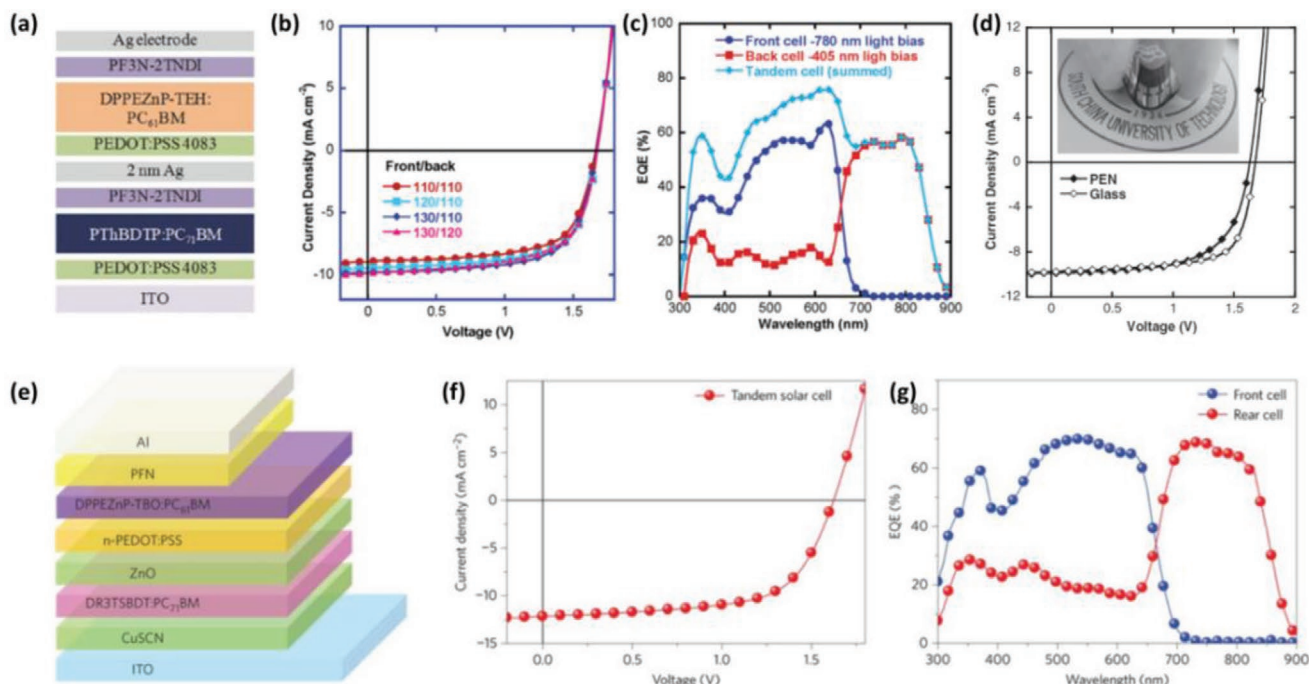


Figure 7. a) Tandem OSC device structure. b) J - V characteristics of double-junction tandem OSC with various thicknesses of front and back cells. c) EQE spectra of the front cell, back cell, and summed EQE spectra of the front and back cells. d) J - V characteristics of glass- and PEN-based tandem OSCs. Inset is the photograph of PEN-based flexible tandem OSC. e) Device architecture of the tandem solar cell. (a-d) reproduced with permission.^[19] Copyright 2016, Wiley-VCH. (e-g) reproduced with permission.^[18] Copyright 2016, Nature Publishing Group.

pairs, rational device optimization route and efficient control of the morphology to improve the crystallinity should be emphasized to further improve the efficiency of non-fullerene-based

small molecule solar cells. In concert with the intrinsic advantages of small molecules that of no batch-to-batch variation, simple synthesis and well-defined structure, small molecule

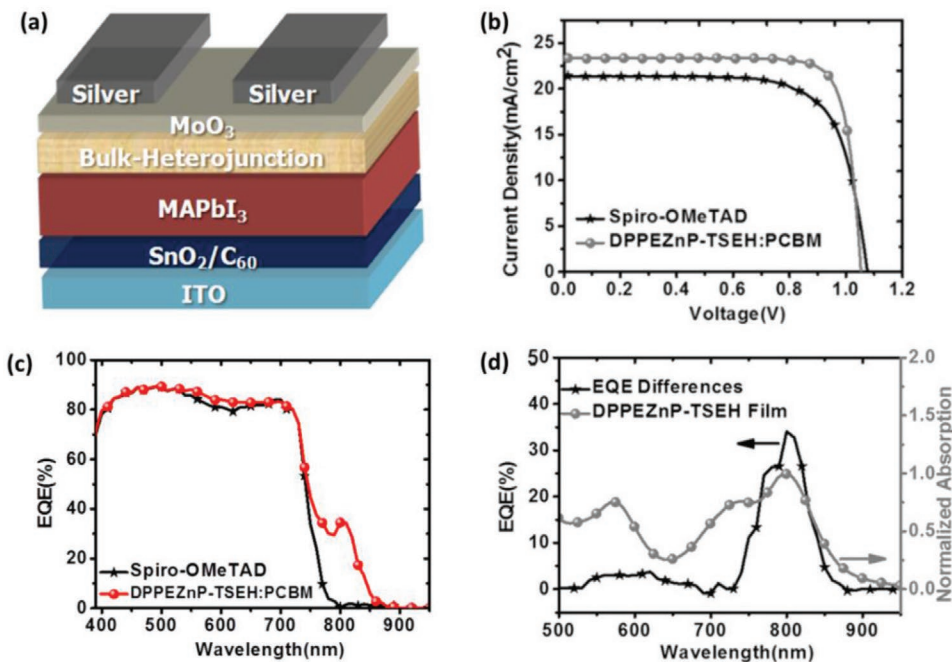


Figure 8. a) OSC-PVSC hybrid solar cells structure. b) J - V curve and c) EQE curve of PVSC and OSC-PVSC hybrid solar cell. d) The differences of EQE between the optimized hybrid solar cell (EQE_{BHJ}) and the optimized control PSC ($EQE_{Spiro-OMeTAD}$), and the absorption of DPPZnP-TSEH in film. Reproduced with permission.^[20] Copyright 2017, Wiley-VCH.

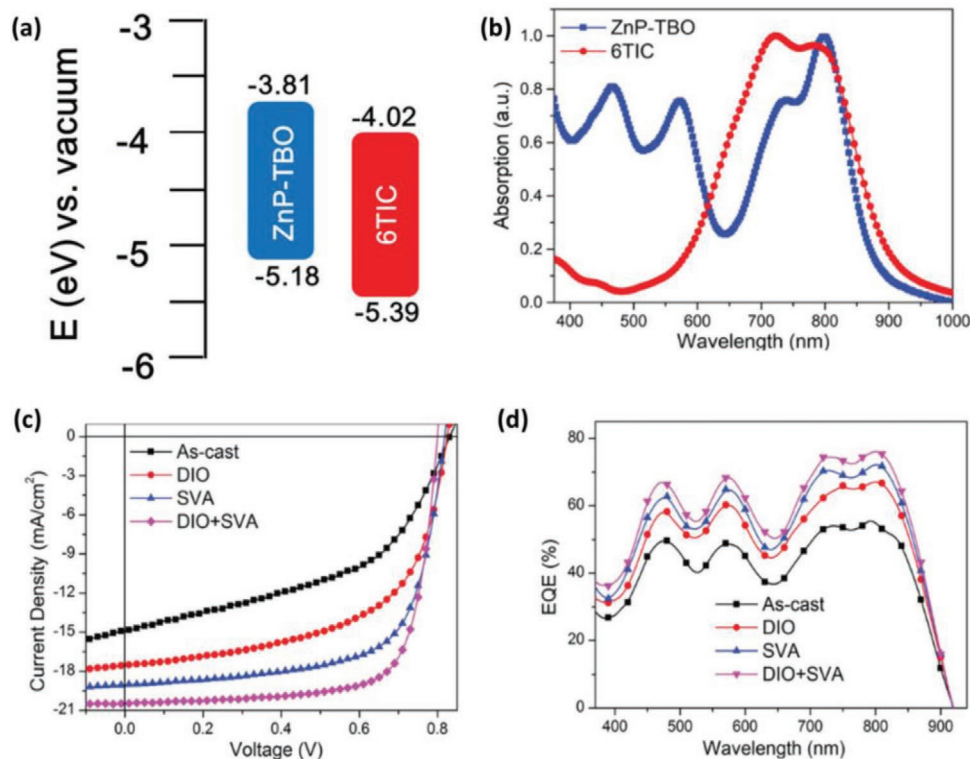


Figure 9. a) Energy-level diagrams for ZnP-TBO and 6TIC. b) UV-vis absorption spectra of ZnP-TBO and 6TIC films. c) J - V curves and d) EQE curves for the devices of the devices with different treatments. Reproduced with permission.^[16] Copyright 2019, Wiley-VCH.

solar cells will become very competitive in the future commercialization of OSCs.^[15,74]

SVA is usually a simple means to tune the morphology to enhance the performance of small molecule solar cells. The origins of the reduction in the V_{oc} , though, need to be understood.^[75] As shown in Figure 10a, devices were made from DPPEZnP-THD and PC61BM. In comparison to the as cast devices, SVA-processed had a significantly reduced V_{oc} . As shown in Figure 10b, this arises from an increased non-radiative recombination and an increased radiative recombination.^[75] From the electroluminescence and EQE, non-radiative recombination and radiative recombination were determined to be 0.31 and 0.23 V, respectively. The as-cast devices, on the other hand, showed values of 0.24 and 0.19 V. Although the SVA-processed devices had a reduced V_{oc} , the higher J_{sc} , and FF led to a PCE of 9.41%.^[75] In this regard, it is important to suppress energetic disorder and/or decrease the non-radiative recombination pathways to get more long-lived charge carriers and thus enhance the open-circuit voltage.

Few studies on the effect of the intermolecular interactions on the morphology and molecular packing adjustment have been performed, thus it deserves more attention in OSC field.^[55] Scanning tunneling microscope (STM) was used to probe the intra- and intermolecular interactions to understand the relationship between morphology adjustment and molecular design on the molecular level.^[76] As shown in Figure 10c for DPPEZnP-TEH, two and even more connected trimeric arrangements formed between tetrameric and trimeric clusters. Defects surrounding these clusters (marked in green)

are evident.^[76] Some irregular cavities, arising from the lack of single molecules and changes in the molecular orientation, are evident. In Figure 10d, DPPEZnP-BzTBO assembled into rows and a 2D network forms. In comparison to DPPEZnP-TEH, the nonplanar structure on the HOPG surface probably led to the bright elliptical spot.^[76] While many questions are opened from such studies, the resolution in the details of the structures will aid in the design of new materials for higher performance.

5. Conclusion and Future Perspectives

Tremendous progress has been made in porphyrin-based OSCs due to the synergetic development of porphyrin materials, device optimization and understanding of morphology. We have synthetically discussed the design and synthetic routes, device optimization, applications, morphological studies, and the related structure-property relationship for porphyrin-based OSCs. Such porphyrin derivatives demonstrate inherent advantages, such as a good extinction coefficient, wide photo-response, and excellent π - π stacking, making porphyrins multifunctional for the use in OSCs and PVSCs. PCEs > 12% with J_{sc} > 20 mA cm⁻² were achieved in non-fullerene small molecule solar cells. In addition, porphyrin-based ternary solar cells, tandem solar cells and flexible solar cells achieved PCEs of 11%, 12.7%, and 10% respectively. All these make DPPEZnP-TRs a family of best low-bandgap donor materials in the OSC field so far. Furthermore, a clear structure-property relationship between morphology and device properties has been established through morphology

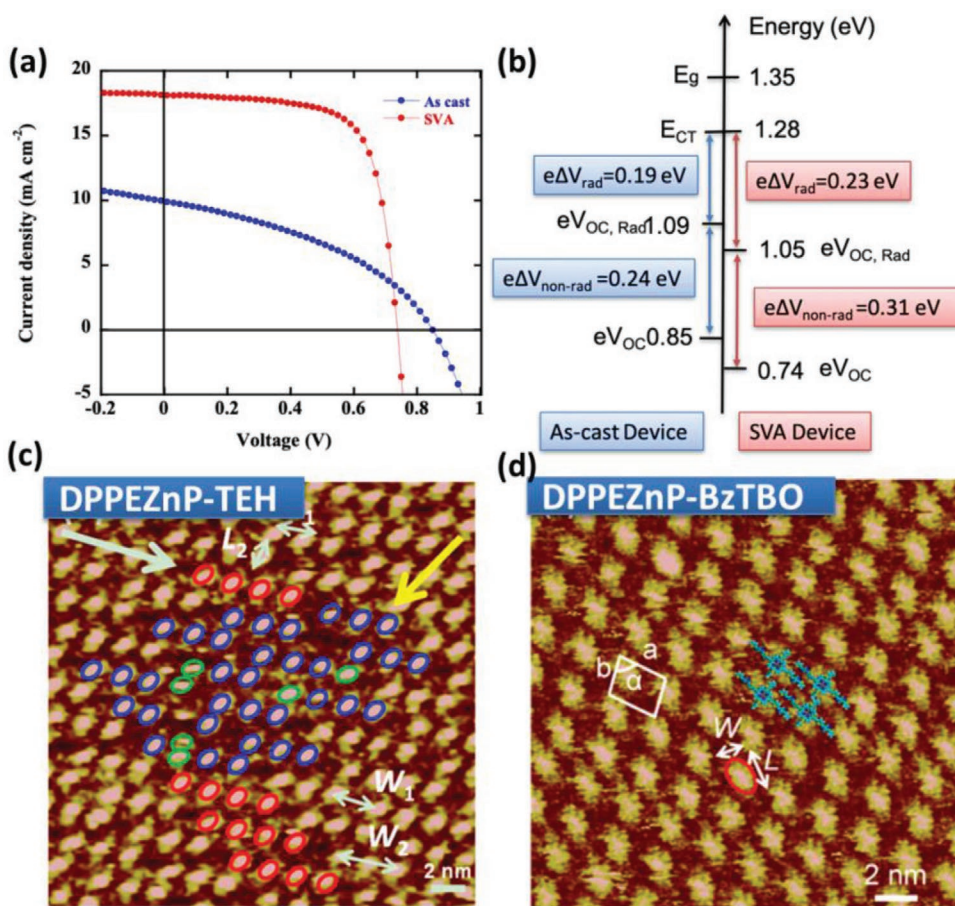


Figure 10. a) J - V curves of small-molecule solar cells with and without SVA. b) Energetics of the OSCs. c) Self-assembled structures of DPPEZnP-TEH networks under the concentration of C3 ($I_{\text{set}} = 230.4$ pA, $V_{\text{bias}} = 721.9$ mV). d) Self-assembly of the DPPEZnP-BzTBO molecule, high-resolution STM image of DPPEZnP-BzTBO self-assemblies ($I_{\text{set}} = 129.1$ pA; $V_{\text{bias}} = 729.8$ mV). (a,b) reproduced with permission.^[75] Copyright 2016, American Chemical Society. (c,d) reproduced with permission.^[76] Copyright 2018, American Chemical Society.

studies. More efficient porphyrin-based OSCs and other applications will emerge by the delicate design of the molecules, comprehensive understanding of morphology and optimization of devices. To push this field forward, we suggest some research guidelines and directions with high potential.

- 1) **Rational design.** More rational design strategies including central metals, side chains, linking units, and end-groups could be considered to further enhance the performance of low bandgap porphyrin materials. For example, porphyrin platinum complexes may further improve the performance of OSCs, since the triplet state can increase the exciton lifetime.^[77]
- 2) **Configuration diversity.** Porphyrins with different configurations could add additional properties to the materials. For example, porphyrin polymers would have the strong mechanical and low bandgap properties.^[66,78] Fused porphyrins could be introduced to improve light absorption, mobility and other properties. Configuration diversity with different functional units could also enable porphyrins to act as acceptors or cathode interface materials.
- 3) **Matched compatibility.** Only PCBM and several non-fullerene acceptors can match well with porphyrin donor materials, likewise, only very few donor materials can match the

few porphyrin-based acceptors. Thus, design and synthesis of new materials well-matched with porphyrin-based materials should keep pace with porphyrin-based materials.

- 4) **In-situ morphology studies.** The kinetics associated with the morphology development and the processing optimization of in the OSC field are not well understood. This requires the use of real-time, in-situ diffraction and scattering studies as solvents, compatibilization agents, and other additives are being removed, so that the interplay between these kinetic processes and the kinetics associated with phase separation and ordering and crystallization are understood and controlled.
- 5) **Additional applications.** Other device applications could be further explored. For example, highly efficient semi-transparent devices and NIR photodetectors could be expected, by taking advantage of the special light absorption properties of some porphyrin materials.

Acknowledgements

K.G. and Y.K. contributed equally to this work. A.K.-Y.J. acknowledges financial support from the Asian Office of Aerospace R&D (FA2386-15-1-4106) and the Office of Naval Research (N00014-17-1-2201, N00014-14-1-0246, N00014-17-1-2260). T.P.R. acknowledges the support of the Office of Naval

Research (N00014-17-1-2241). P.X.B. thanks the National Natural Science Foundation of China (51773065 and 51473053), the International Science and Technology Cooperation Program of China (2013DFG52740), National Key Research and Development Program of China (2017YFA0206602), and the Fundamental Research Funds for the Central Universities.

Conflict of Interest

The authors declare no conflict of interest.

Keywords

organic solar cells, porphyrin, solar cell morphology

Received: October 12, 2019

Revised: April 6, 2020

Published online: June 25, 2020

- [1] P. Cheng, G. Li, X. Zhan, Y. Yang, *Nat. Photonics* **2018**, *12*, 131.
- [2] J. Hou, O. Inganäs, R. H. Friend, F. Gao, *Nat. Mater.* **2018**, *17*, 119.
- [3] C. Yan, S. Barlow, Z. Wang, H. Yan, A. K.-Y. Jen, S. R. Marder, X. Zhan, *Nat. Rev. Mater.* **2018**, *3*, 18003.
- [4] J. Zhang, H. S. Tan, X. Guo, A. Facchetti, H. Yan, *Nat. Energy* **2018**, *3*, 720.
- [5] L. Meng, Y. Zhang, X. Wan, C. Li, X. Zhang, Y. Wang, X. Ke, Z. Xiao, L. Ding, R. Xia, H.-L. Yip, Y. Cao, Y. Chen, *Science* **2018**, *361*, 1094.
- [6] J. Yuan, Y. Zhang, L. Zhou, G. Zhang, H.-L. Yip, T.-K. Lau, X. Lu, C. Zhu, H. Peng, P. A. Johnson, M. Leclerc, Y. Cao, J. Ulanski, Y. Li, Y. Zou, *Joule* **2019**, *3*, 1.
- [7] Z. Xiao, X. Jia, L. Ding, *Sci. Bull.* **2017**, *62*, 1562.
- [8] Y. Cui, H. Yao, J. Zhang, T. Zhang, Y. Wang, L. Hong, K. Xian, B. Xu, S. Zhang, J. Peng, Z. Wei, F. Gao, J. Hou, *Nat. Commun.* **2019**, *10*, 2515.
- [9] X. Xu, K. Feng, Z. Bi, W. Ma, G. Zhang, Q. Peng, *Adv. Mater.* **2019**, *31*, 1901872.
- [10] T. Yan, W. Song, J. Huang, R. Peng, L. Huang, Z. Ge, *Adv. Mater.* **2019**, *31*, 1902210.
- [11] L. Dou, Y. Liu, Z. Hong, G. Li, Y. Yang, *Chem. Rev.* **2015**, *115*, 12633.
- [12] J. Kesters, P. Verstappen, M. Kelchtermans, L. Lutsen, D. Vanderzande, W. Maes, *Adv. Energy Mater.* **2015**, *5*, 1500218.
- [13] A. Mahmood, J.-Y. Hu, B. Xiao, A. Tang, X. Wang, E. Zhou, *J. Mater. Chem. A* **2018**, *6*, 16769.
- [14] K. Gao, L. Li, T. Lai, L. Xiao, Y. Huang, F. Huang, J. Peng, Y. Cao, F. Liu, T. P. Russell, R. A. Janssen, X. Peng, *J. Am. Chem. Soc.* **2015**, *137*, 7282.
- [15] K. Gao, S. B. Jo, X. Shi, L. Nian, M. Zhang, Y. Kan, F. Lin, B. Kan, B. Xu, Q. Rong, L. Shui, F. Liu, X. Peng, G. Zhou, Y. Cao, A. K.-Y. Jen, *Adv. Mater.* **2019**, *31*, 1807842.
- [16] L. Nian, K. Gao, Y. Jiang, Q. Rong, X. Hu, D. Yuan, F. Liu, X. Peng, T. P. Russell, G. Zhou, *Adv. Mater.* **2017**, *29*, 1700616.
- [17] L. Nian, K. Gao, F. Liu, Y. Kan, X. Jiang, L. Liu, Z. Xie, X. Peng, T. P. Russell, Y. Ma, *Adv. Mater.* **2016**, *28*, 8184.
- [18] M. Li, K. Gao, X. Wan, Q. Zhang, B. Kan, R. Xia, F. Liu, X. Yang, H. Feng, W. Ni, Y. Wang, J. Peng, H. Zhang, Z. Liang, H.-L. Yip, X. Peng, Y. Cao, Y. Chen, *Nat. Photonics* **2017**, *11*, 85.
- [19] K. Zhang, K. Gao, R. Xia, Z. Wu, C. Sun, J. Cao, L. Qian, W. Li, S. Liu, F. Huang, X. Peng, L. Ding, H. L. Yip, Y. Cao, *Adv. Mater.* **2016**, *28*, 4817.
- [20] K. Gao, Z. Zhu, B. Xu, S. B. Jo, Y. Kan, X. Peng, A. K. Jen, *Adv. Mater.* **2017**, *29*, 1703980.
- [21] B. J. Littler, M. A. Miller, C.-H. Hung, R. W. Wagner, D. F. O'Shea, P. D. Boyle, J. S. Lindsey, *J. Org. Chem.* **1999**, *64*, 1391.
- [22] B. J. Littler, Y. Ciringh, J. S. Lindsey, *J. Org. Chem.* **1999**, *64*, 2864.
- [23] W. L. Leong, G. C. Welch, L. G. Kaake, C. J. Takacs, Y. Sun, G. C. Bazan, A. J. Heeger, *Chem. Sci.* **2012**, *3*, 2103.
- [24] D. Dolphin, *J. Heterocycl. Chem.* **1970**, *7*, 275.
- [25] D. Veldman, S. C. Meskers, R. A. Janssen, *Adv. Funct. Mater.* **2009**, *19*, 1939.
- [26] Y. Wang, D. Qian, Y. Cui, H. Zhang, J. Hou, K. Vandewal, T. Kirchartz, F. Gao, *Adv. Energy Mater.* **2018**, *8*, 1801352.
- [27] K. Gao, J. Miao, L. Xiao, W. Deng, Y. Kan, T. Liang, C. Wang, F. Huang, J. Peng, Y. Cao, F. Liu, T. P. Russell, H. Wu, X. Peng, *Adv. Mater.* **2016**, *28*, 4727.
- [28] T. Liang, L. Xiao, C. Liu, K. Gao, H. Qin, Y. Cao, X. Peng, *Org. Electron.* **2016**, *29*, 127.
- [29] T. Liang, L. Xiao, K. Gao, W. Xu, X. Peng, Y. Cao, *ACS Appl. Mater. Interfaces* **2017**, *9*, 7131.
- [30] K. Gao, L. Xiao, Y. Kan, B. Yang, J. Peng, Y. Cao, F. Liu, T. P. Russell, X. Peng, *J. Mater. Chem. C* **2016**, *4*, 3843.
- [31] H. Wang, L. Xiao, L. Yan, S. Chen, X. Zhu, X. Peng, X. Wang, W. K. Wong, W. Y. Wong, *Chem. Sci.* **2016**, *7*, 4301.
- [32] L. Xiao, S. Chen, K. Gao, X. Peng, F. Liu, Y. Cao, W. Y. Wong, W. K. Wong, X. Zhu, *ACS Appl. Mater. Interfaces* **2016**, *8*, 30176.
- [33] X. Zhou, W. Tang, P. Bi, L. Yan, X. Wang, W.-K. Wong, X. Hao, B. S. Ong, X. Zhu, *J. Mater. Chem. A* **2018**, *6*, 14675.
- [34] S. Chen, L. Yan, L. Xiao, K. Gao, W. Tang, C. Wang, C. Zhu, X. Wang, F. Liu, X. Peng, W.-K. Wong, X. Zhu, *J. Mater. Chem. A* **2017**, *5*, 25460.
- [35] T. Lai, X. Chen, L. Xiao, L. Zhang, T. Liang, X. Peng, Y. Cao, *Chem. Commun.* **2017**, *53*, 5113.
- [36] T. Lai, L. Xiao, K. Deng, T. Liang, X. Chen, X. Peng, Y. Cao, *ACS Appl. Mater. Interfaces* **2018**, *10*, 668.
- [37] L. Xiao, T. Lai, X. Liu, F. Liu, T. P. Russell, Y. Liu, F. Huang, X. Peng, Y. Cao, *J. Mater. Chem. A* **2018**, *6*, 18469.
- [38] C. V. Kumar, L. Cabau, E. N. Koukaras, A. Sharma, G. D. Sharma, E. Palomares, *J. Mater. Chem. A* **2015**, *3*, 16287.
- [39] S. Arrechea, A. Molina-Ontoria, A. Aljarilla, P. de la Cruz, F. Langa, L. Echegoyen, *Dyes Pigm.* **2015**, *121*, 109.
- [40] G. Morán, S. Arrechea, P. de la Cruz, V. Cuesta, S. Biswas, E. Palomares, G. D. Sharma, F. Langa, *J. Mater. Chem. A* **2016**, *4*, 11009.
- [41] S. Arrechea, A. Aljarilla, P. de la Cruz, E. Palomares, G. D. Sharma, F. Langa, *Nanoscale* **2016**, *8*, 17953.
- [42] S. Arrechea, A. Aljarilla, P. de la Cruz, M. K. Singh, G. D. Sharma, F. Langa, *J. Mater. Chem. C* **2017**, *5*, 4742.
- [43] V. Cuesta, M. Vartanian, P. de la Cruz, R. Singhal, G. D. Sharma, F. Langa, *J. Mater. Chem. A* **2017**, *5*, 1057.
- [44] Y. Zhen, H. Tanaka, K. Harano, S. Okada, Y. Matsuo, E. Nakamura, *J. Am. Chem. Soc.* **2015**, *137*, 2247.
- [45] K. Ogumi, T. Nakagawa, H. Okada, R. Sakai, H. Wang, Y. Matsuo, *J. Mater. Chem. A* **2017**, *5*, 23067.
- [46] A. Zhang, C. Li, F. Yang, J. Zhang, Z. Wang, Z. Wei, W. Li, *Angew. Chem., Int. Ed.* **2017**, *56*, 2694.
- [47] W. T. Hadmojo, D. Yim, S. Sinaga, W. Lee, D. Y. Ryu, W.-D. Jang, I. H. Jung, S.-Y. Jang, *ACS Sustainable Chem. Eng.* **2018**, *6*, 5306.
- [48] L. Bucher, N. Desbois, E. N. Koukaras, C. H. Devillers, S. Biswas, G. D. Sharma, C. P. Gros, *J. Mater. Chem. A* **2018**, *6*, 8449.
- [49] Y. Lu, Z. Xiao, Y. Yuan, H. Wu, Z. An, Y. Hou, C. Gao, J. Huang, *J. Mater. Chem. C* **2013**, *1*, 630.
- [50] X. Liu, Y. Li, K. Ding, S. Forrest, *Phys. Rev. Appl.* **2019**, *11*, 024060.
- [51] D. Qian, Z. Zheng, H. Yao, W. Tress, T. R. Hopper, S. Chen, S. Li, J. Liu, S. Chen, J. Zhang, X.-K. Liu, B. Gao, L. Ouyang, J. Yingzhi, G. Pozina, I. A. Buyanova, W. M. Chen, O. Inganäs, V. Coropceanu, J.-L. Bredas, H. Yan, J. Hou, F. Zhang, A. A. Bakulin, F. Gao, *Nat. Mater.* **2018**, *17*, 703.

- [52] H. B. Naveed, W. Ma, *Joule* **2018**, 2, 621.
- [53] L. Ye, B. A. Collins, X. Jiao, J. Zhao, H. Yan, H. Ade, *Adv. Energy Mater.* **2018**, 8, 1703058.
- [54] L. Ye, H. Hu, M. Ghasemi, T. Wang, B. A. Collins, J.-H. Kim, K. Jiang, J. H. Carpenter, H. Li, Z. Li, T. McAfee, J. Zhao, X. Chen, H. L. Y. Lai, T. Ma, J.-L. Bredas, H. Yan, H. Ade, *Nat. Mater.* **2018**, 17, 253.
- [55] Z. Luo, H. Bin, T. Liu, Z. G. Zhang, Y. Yang, C. Zhong, B. Qiu, G. Li, W. Gao, D. Xie, *Adv. Mater.* **2018**, 30, 1706124.
- [56] D. Liu, Q. Zhu, C. Gu, J. Wang, M. Qiu, W. Chen, X. Bao, M. Sun, R. Yang, *Adv. Mater.* **2016**, 28, 8490.
- [57] K. Gao, W. Deng, L. Xiao, Q. Hu, Y. Kan, X. Chen, C. Wang, F. Huang, J. Peng, H. Wu, X. Peng, Y. Cao, T. P. Russell, F. Liu, *Nano Energy* **2016**, 30, 639.
- [58] J. Zhang, Y. Zhang, J. Fang, K. Lu, Z. Wang, W. Ma, Z. Wei, *J. Am. Chem. Soc.* **2015**, 137, 8176.
- [59] Q. An, F. Zhang, J. Zhang, W. Tang, Z. Deng, B. Hu, *Energy Environ. Sci.* **2016**, 9, 281.
- [60] L. Gao, Z. G. Zhang, L. Xue, J. Min, J. Zhang, Z. Wei, Y. Li, *Adv. Mater.* **2016**, 28, 1884.
- [61] W.-Y. Tan, K. Gao, J. Zhang, L.-L. Chen, S.-P. Wu, X.-F. Jiang, X.-B. Peng, Q. Hu, F. Liu, H.-B. Wu, Y. Cao, X.-H. Zhu, *Sol. RRL* **2017**, 1, 1600003.
- [62] L. Xiao, T. Liang, K. Gao, T. Lai, X. Chen, F. Liu, T. P. Russell, F. Huang, X. Peng, Y. Cao, *ACS Appl. Mater. Interfaces* **2017**, 9, 29917.
- [63] X. Xu, T. Yu, Z. Bi, W. Ma, Y. Li, Q. Peng, *Adv. Mater.* **2018**, 30, 1703973.
- [64] S. Li, L. Zhan, F. Liu, J. Ren, M. Shi, C. Z. Li, T. P. Russell, H. Chen, *Adv. Mater.* **2018**, 30, 1705208.
- [65] Y. Lin, J. Wang, Z. G. Zhang, H. Bai, Y. Li, D. Zhu, X. Zhan, *Adv. Mater.* **2015**, 27, 1170.
- [66] D. Chen, J. Yao, L. Chen, J. Yin, R. Lv, B. Huang, S. Liu, Z. G. Zhang, C. Yang, Y. Chen, *Angew. Chem., Int. Ed.* **2018**, 57, 4580.
- [67] Q. Fan, Y. Wang, M. Zhang, B. Wu, X. Guo, Y. Jiang, W. Li, B. Guo, C. Ye, W. Su, J. Fang, X. Ou, F. Liu, Z. Wei, T. C. Sum, T. P. Russell, Y. Li, *Adv. Mater.* **2018**, 30, 1704546.
- [68] T. Liu, L. Huo, S. Chandrabose, K. Chen, G. Han, F. Qi, X. Meng, D. Xie, W. Ma, Y. Yi, J. M. Hodgkiss, F. Liu, J. Wang, C. Yang, Y. Sun, *Adv. Mater.* **2018**, 30, 1707353.
- [69] X. Long, Z. Ding, C. Dou, J. Zhang, J. Liu, L. Wang, *Adv. Mater.* **2016**, 28, 6504.
- [70] Y. Cui, H. Yao, L. Hong, T. Zhang, Y. Xu, K. Xian, B. Gao, J. Qin, J. Zhang, Z. Wei, J. Hou, *Adv. Mater.* **2019**, 31, 1808356.
- [71] J. Guo, H. Bin, W. Wang, B. Chen, J. Guo, R. Sun, Z.-G. Zhang, X. Jiao, Y. Li, J. Min, *J. Mater. Chem. A* **2018**, 6, 15675.
- [72] H. Li, Y. Zhao, J. Fang, X. Zhu, B. Xia, K. Lu, Z. Wang, J. Zhang, X. Guo, Z. Wei, *Adv. Energy Mater.* **2018**, 8, 1702377.
- [73] N. Liang, D. Meng, Z. Ma, B. Kan, X. Meng, Z. Zheng, W. Jiang, Y. Li, X. Wan, J. Hou, W. Ma, Y. Chen, Z. Wang, *Adv. Energy Mater.* **2017**, 7, 1601664.
- [74] Z. Zhou, S. Xu, J. Song, Y. Jin, Q. Yue, Y. Qian, F. Liu, F. Zhang, X. Zhu, *Nat. Energy* **2018**, 3, 952.
- [75] W. Deng, K. Gao, J. Yan, Q. Liang, Y. Xie, Z. He, H. Wu, X. Peng, Y. Cao, *ACS Appl. Mater. Interfaces* **2018**, 10, 8141.
- [76] Y. Qian, B. Tu, K. Gao, T. Liang, X. Zhu, B. Liu, W. Duan, X. Peng, Q. Fang, Y. Geng, Q. Zeng, *Langmuir* **2018**, 34, 11952.
- [77] Y. Jin, Y. Zhang, Y. Liu, J. Xue, W. Li, J. Qiao, F. Zhang, *Adv. Mater.* **2019**.
- [78] X. Huang, C. Zhu, S. Zhang, W. Li, Y. Guo, X. Zhan, Y. Liu, Z. Bo, *Macromolecules* **2008**, 41, 6895.